Chapter 4

Results and Discussion

In this chapter, the results and discussion are presented. It includes the results from MOCVD, electrochemical oxidation and also the kinetic investigation of electrochemical oxidation.

4.1 Preparation of specific electrodes

4.1.1 Treatment of substrates

To improve the surface roughness of substrates for better adhesion of deposited films, the substrates need to be etched by the appropriating acid. In case of Ta substrate, the 40% HF was used as etching reagent. After etching, the average surface roughness of Ta substrates was increased. The Ta surface roughness progressed slowly comparing with Ti substrates etched by hot-HCl for 1 hr. Figures 4-1 and 4-2 represent the surface profile of 24 hr etched Ta in HF and 1 hr etched Ti substrate in hot-HCl. Although, Ta substrate was etched by stronger acid as HF, but the Ta surface roughness was still smaller than Ti surface because the chemical stability of Ta is much higher than that of Ti substrate. The average surface roughness of 1 hr hot-HCl etched Ti was 414 nm, while the average surface roughness of Ta substrates at various etching time is less than 300 nm presented in Figure 4-3. The increasing surface area was confirmed by the observation with SEM in Figure 4-4.

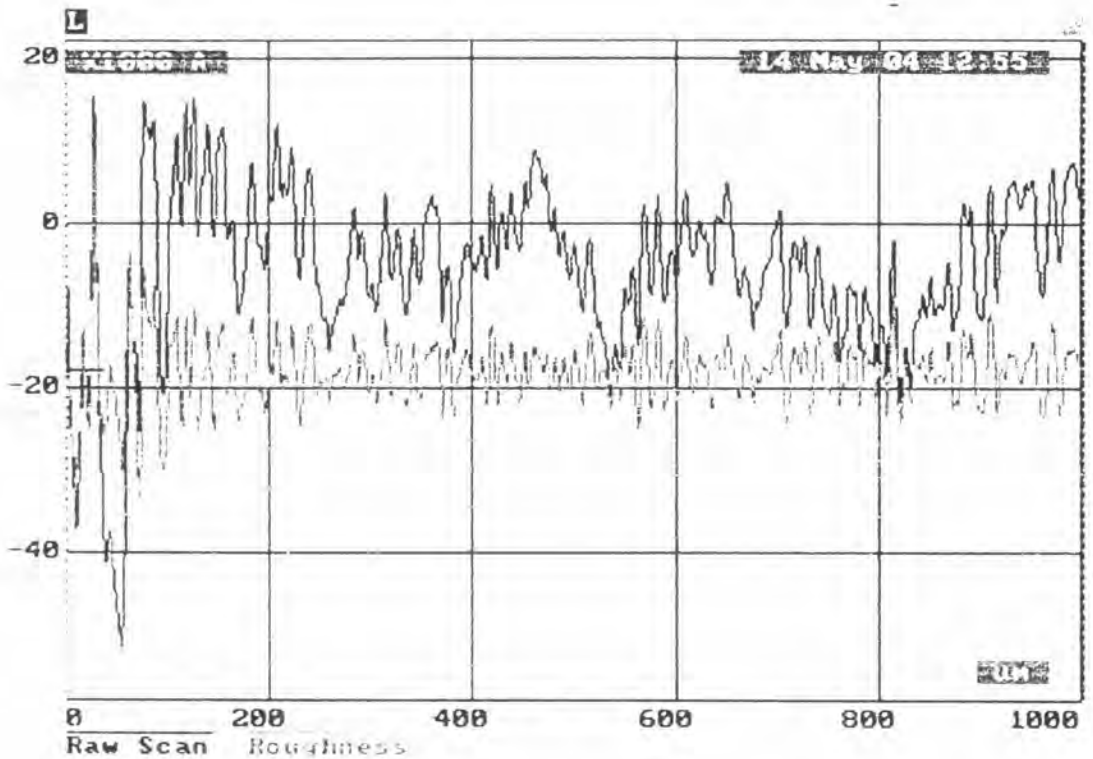

Figure 4-1 Roughness profile of 24 hr HF etched Ta substrate

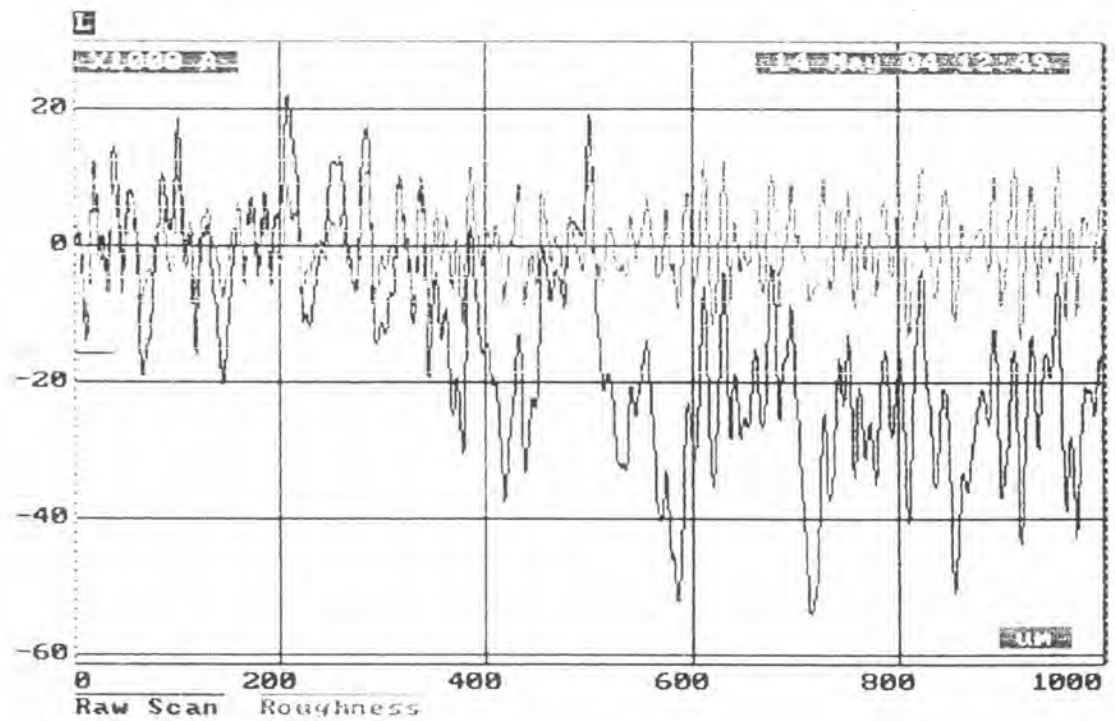

Figure 4-2 Roughness profile of 1 hr hot-HCl etched Ti substrate

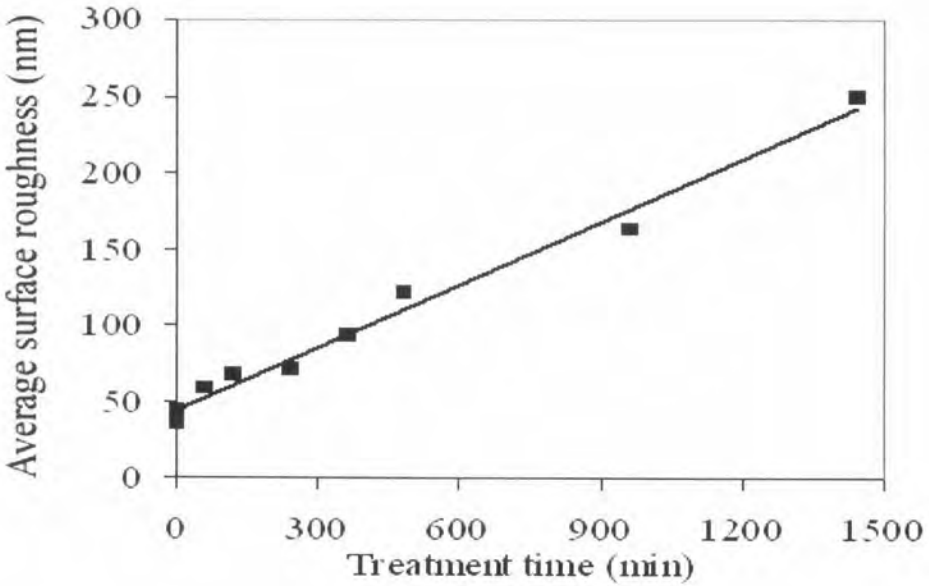

Figure 4-3 The average surface roughness of Ta substrates with various etching time by HF

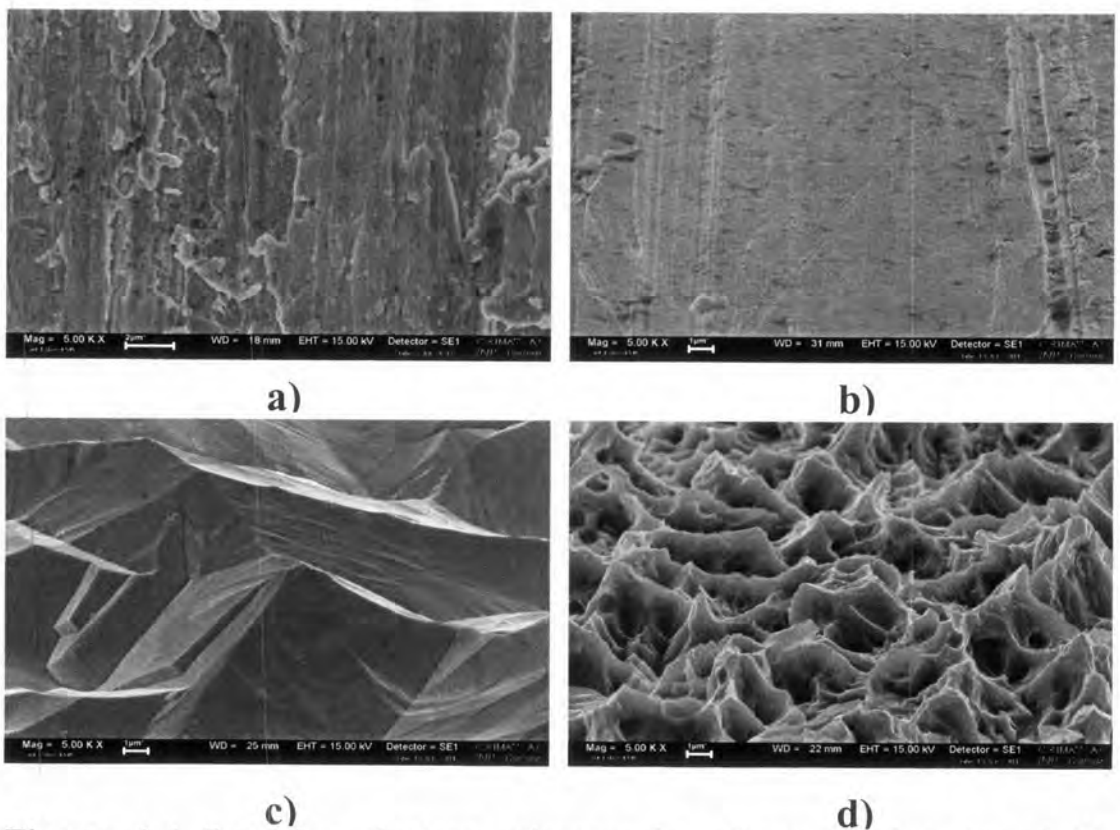

Figure 4-4 Scanning electron micrographs of some substrates a) Ta without etching, b) Ta with 1 hr etching, c) Ta with 24 hr etching and d) Ti with 1 hr etching

4.1.2 Deposition of TiO_2 by spray coating

The deposition of TiO_2 by spray coating produced the uniform and good coverage TiO_2 coating over SUS 316L substrate. However, the TiO_2 stripping was observed in a few minutes when it was used as anode in an electrochemical oxidation of wastewater (Chulalongkorn University effluent). It may be because that the TiO_2 layer had high porosity and low adhesion. The oxidation of SUS 316L substrate was occurred due to the attack of wastewater at high potential.

Because of a very short service life of TiO_2/SUS 316L and low adhesion of TiO_2 layer, the TiO_2/SUS 316L was unsuitable to use as electrode for wastewater treatment by electrochemical oxidation.

4.1.3 Deposition of SnO_2 by spray pyrolysis

The deposition of SnO_2 by spray pyrolysis was investigated at 500 °C in ambient atmosphere. Due to the uncontrolled drop size of precursor solution sprayed by simple atomizer, the SnO_2 film is resulted in inhomogeneous coating. The unregulated surface temperature made some precursor incompletely reacted with oxygen. Some precursor was observed on the substrate surface.

Due to its inhomogeneous coating of SnO_2 film by spray pyrolysis, it could be mentioned that the spray pyrolysis technique was inappropriate to use as the method for production of SnO_2 specific electrode.

4.1.4 Deposition of IrO_2 by MOCVD

The deposition of IrO_2 film with presence of O_2 was investigated at 400 °C and 25 Torr. The $O_2/Ir(acac)_3$ molar ratios were 11,000 and 17,000 on Si wafer and Ti substrate.

The effect of $O_2/Ir(acac)_3$ molar ratio on IrO_2 film growth rate is presented in Figure 4-5. The IrO_2 film growth rate increased to the maximum growth rate at 2.5 cm from the entrance of reactor, but it decreased immediately downstream. When the $O_2/Ir(acac)_3$ molar ratio was 17,000, the maximum growth rate was 1.9 nm/min and reduced to 0.9 nm/min at 7.5 cm from the entrance. However, the IrO_2 growth rate was undetected after passing into the reactor more than 12.5 cm. Although $O_2/Ir(acac)_3$ ratio was decreased to 11,000, the maximum IrO_2 growth rate was 2.9 nm/min still at 2.5 cm position and was reduced to 1.9 nm/nim at 7.5 cm from the entrance of the reactor.

The comparison of IrO_2 growth rate when $O_2/Ir(acac)_3$ molar ratio was decreased from 17,000 to 11,000. It was found that the higher Ir source ratio is the higher IrO_2 film growth rate obtains due to its higher Ir precursor concentration in feed vapor. However, decreasing $O_2/Ir(acac)_3$ molar ratio could not improve the deposition in more homogeneous and uniform deposition; the IrO_2 thickness profile was still similar. It was caused by the $Ir(acac)_3$ consumed and deposited immediately after entering to the reactor only a few centimeters. The $Ir(acac)_3$ reacted with mixed oxygen at lower temperature than desired deposition temperature. It was confirmed by the deposition of Ir film at the 1.0-1.5 cm from the entrance of reactor that lower temperature was observed in some experiments. However, the IrO_2 film growth rate was significantly affected by $O_2/Ir(acac)_3$ molar ratio.

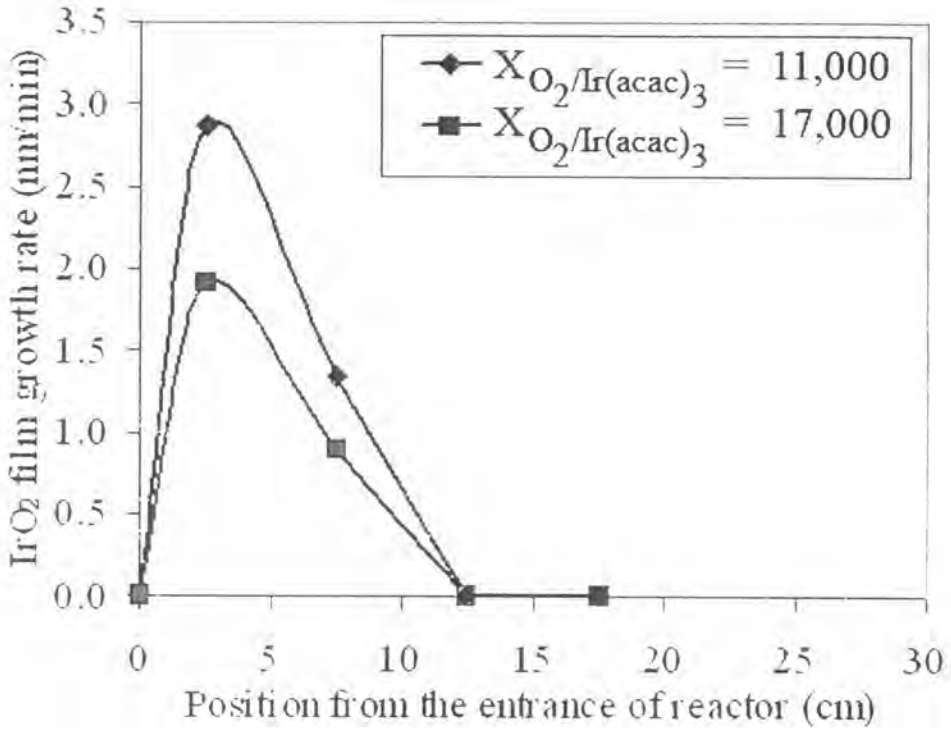

Figure 4-5 Effect of $O_2/Ir(acac)_3$ molar ratio on IrO_2 film growth rate at 400 °C and 25 Torr

The $O_2/Ir(acac)_3$ molar ratio not only affected on IrO_2 film growth rate, but it also affected on the microstructure of IrO_2 film. The X-ray diffraction of IrO_2 film deposited at 2 cm from the entrance of reactor was presented in Figure 4-6. It was found that when decreased the $O_2/Ir(acac)_3$ molar ratio from 17,000 to 11,000, the peak of (101) orientation was decreased, but the peak of (110) orientation was outstanding, while the other peaks were not quite changed.

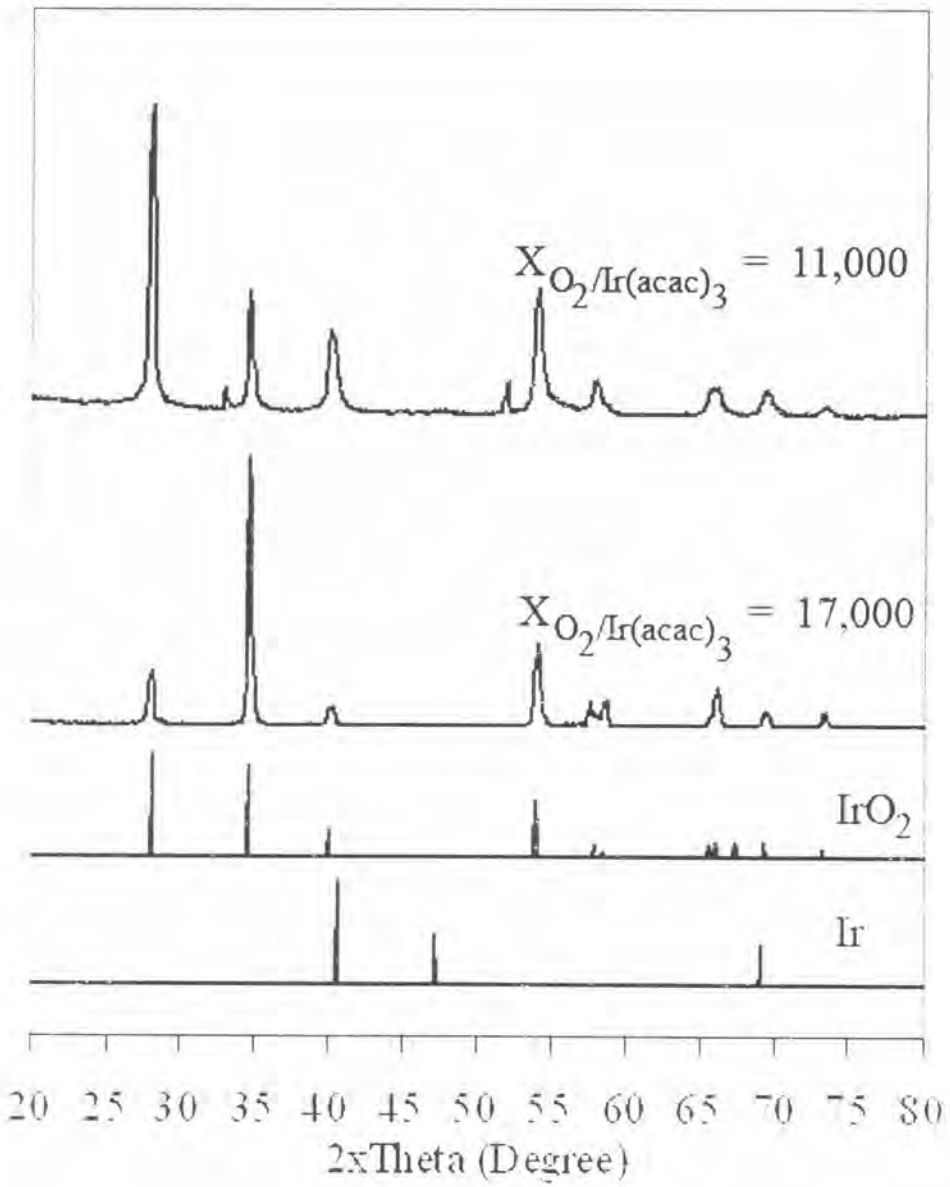

Figure 4-6 X-Ray diffraction of IrO_2 coated Si wafer

The effect of $O_2/Ir(acac)_3$ ratio was confirmed by SEM images in Figure 4-7, the columnar growth of IrO_2 with (101) orientation was observed when $O_2/Ir(acac)_3$ molar ratio was 17,000, while the dense IrO_2 film with (110) orientation was observed at molar ratio of 11,000.

Although, the IrO_2 film had homogeneous microstructure and good coverage on Si wafer, when Si wafer was substituted by actual Ti

substrate, the gradient deposition of IrO_2 film was observed. It was occurred due to the low volatility and difficult to control mass transfer of $Ir(acac)_3$.

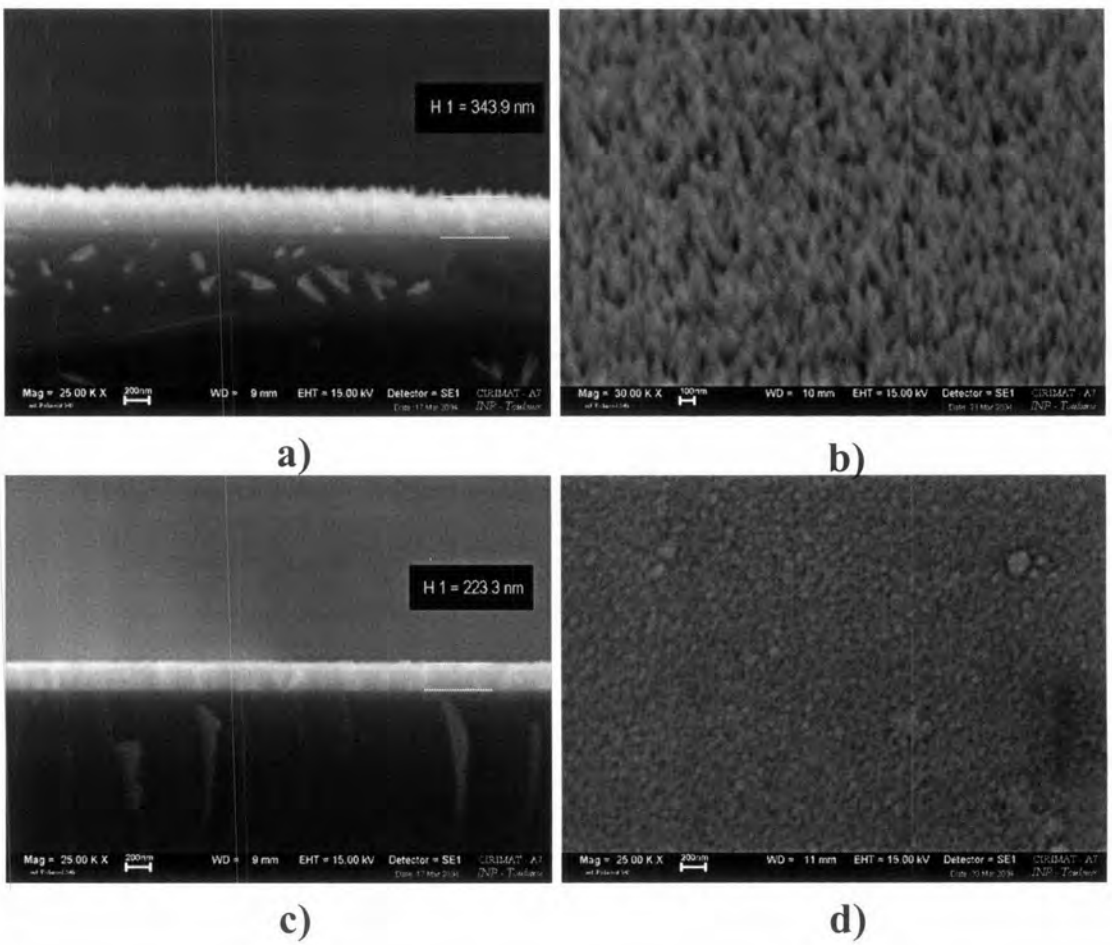

Figure 4-7 Cross-sectional and surface microstructure of IrO_2 film over Si wafer; a-b) $O_2/Ir(acac)_3$ molar ratio of 17,000 and c-d) $O_2/Ir(acac)_3$ molar ratio of 11,000

4.1.5 Deposition of Ir by MOCVD

Deposition of Ir film by using (MeCp)Ir(COD) as precursor with MOCVD could be operated at various condition as reported in some literatures [4, 46]. In this work, the deposition of Ir film with the presence of O_2 was investigated. It was found that the deposition of Ir film was strongly affected by deposition temperature and oxygen content in feed vapor mixture.

The effect of deposition temperature on the Ir film deposition is represented in Figure 4-8. At high O_2/(MeCp)Ir(COD) molar ratio in feed gas mixture (1491±89), the increasing deposition temperature from 300 to 325 and 350 °C has significantly affected on the deposition area of Ir film. The deposition area of Ir film was decreased from 13 to 11 and 9.75 cm from the entrance of the reactor, respectively. It agrees with some results in Figure 4-9, the growth rate of Ir film was very high at a few centimeters nearby the entrance of the reactor. However, the Ir film growth rate rapidly decreased downstream. It may be affected by at high deposition temperature, the precursor had higher internal energy. So, the precursor reacted with co-reactive gas and consumed immediately in a few centimeter from the entrance.

The effect of oxygen content in feed vapor mixture on deposition area was represented in Figure 4-10. At O_2/(MeCp)Ir(COD) molar ratio of 1545, (MeCp)Ir(COD) was completely decomposed and the yield of the Ir deposited film in the reactor was nearly 100%. However, the Ir film was deposited only at the entrance of the reactor and the gradient growth rate was observed because the system was very high reactivity when oxygen content was too high and the precursor consumed immediately. In contrast to low O_2/(MeCp)Ir(COD) molar ratio of 125, the reactivity of

the system was decreased by reducing O_2/(MeCp)Ir(COD) molar ratio. In this case, the Ir film deposited uniformly over several centimeters distance through the reactor. It was confirmed by Figure 4-11, the growth rate increased to the maximum film growth rate at around 10 cm from the entrance before decreased rapidly downstream

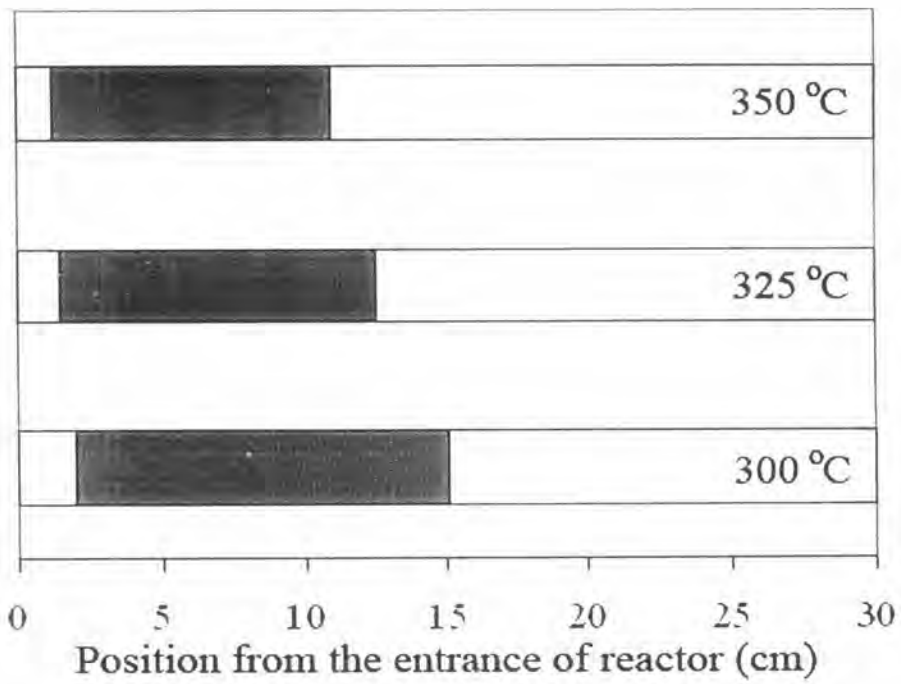

Figure 4-8 Effect of deposition temperature on deposition area of Ir film at 12 Torr and O_2/(MeCp)Ir(COD) molar ratio of 1491±89, (▩) deposition area

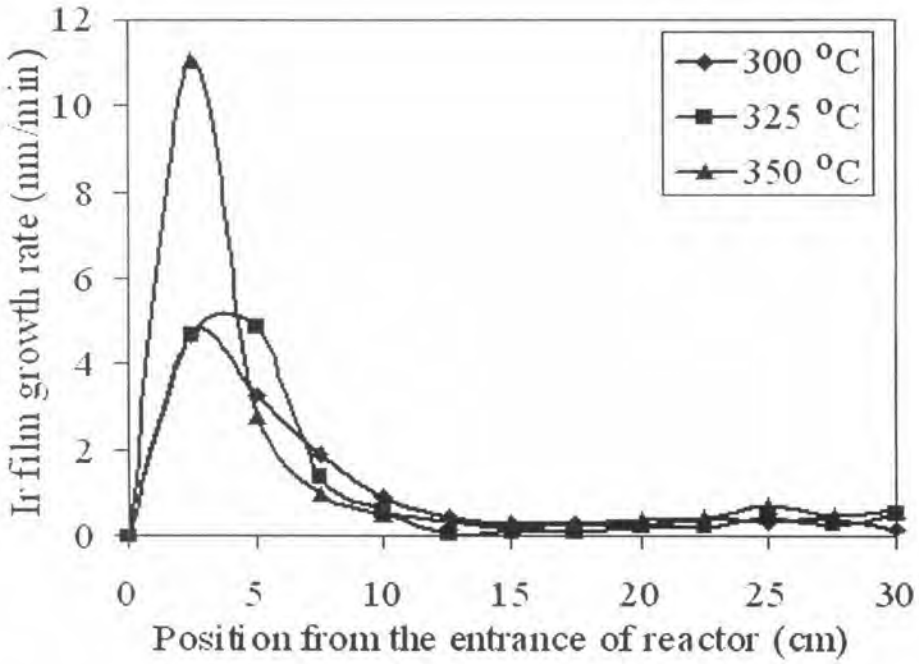

Figure 4-9 Effect of deposition temperature on Ir film growth rate at 12 Torr and O_2/(MeCp)Ir(COD) molar ratio of 1491±89

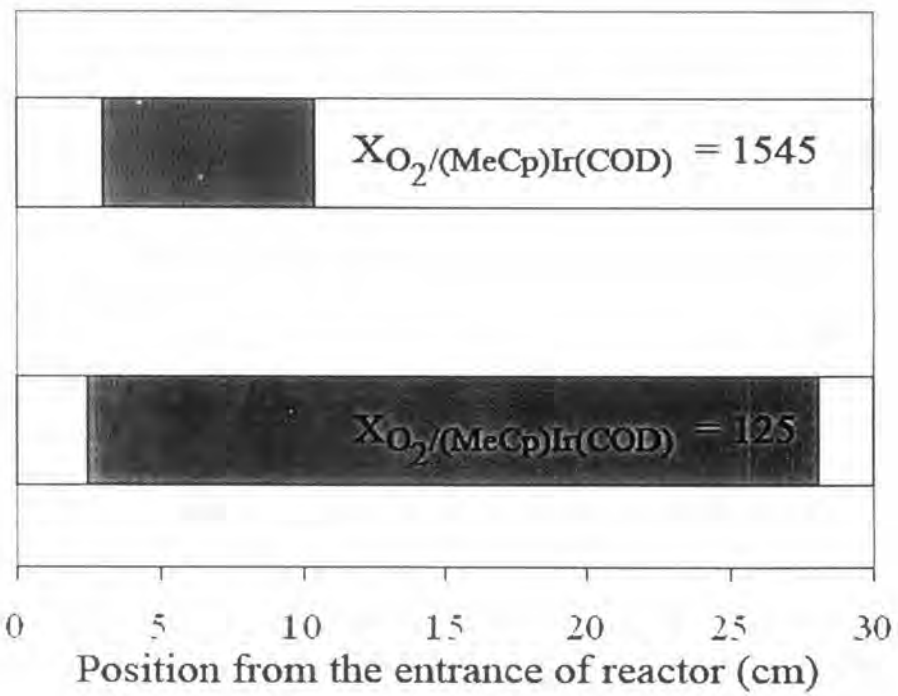

Figure 4-10 Effect of oxygen content in feed gas mixture on deposition area of Ir film at 300 °C and 12 Torr, (▩) deposition area

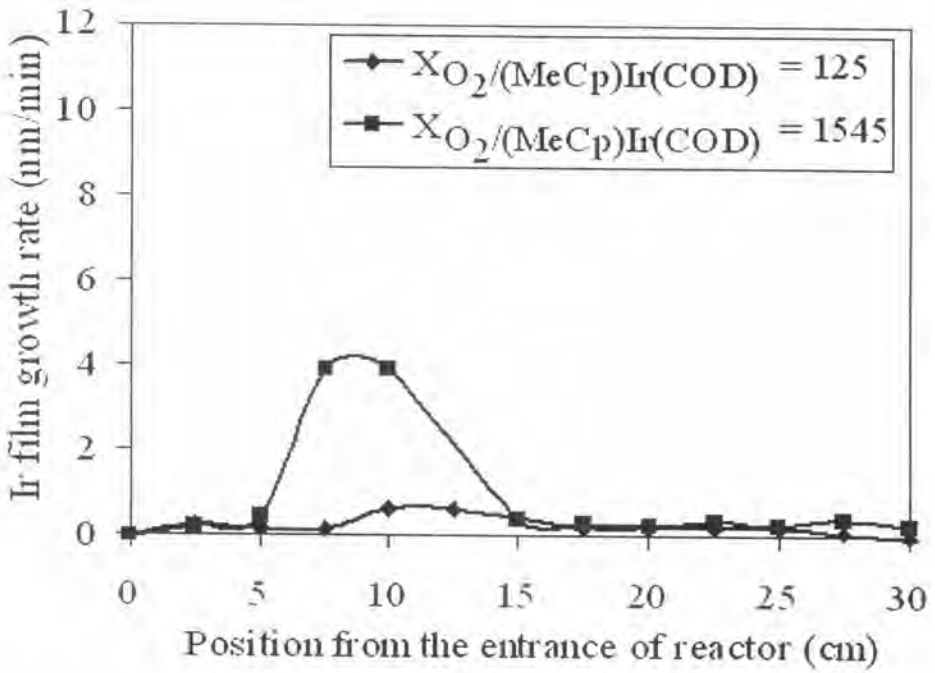

Figure 4-11 Effect of oxygen molar ratio on Ir film growth rate at 300 °C and 12 Torr

Figure 4-12 represents the SEM images of Ir film on Si wafer and hot-HCl treated Ti substrate. The micrographs present the very smooth, homogeneous and good coverage deposition of Ir film. The Ir deposition also has very high purity. It could be confirmed by the XRD spectra in Figure 4-13. From these results, we could say that the deposited Ir film is very good to be used as the protective layer for SnO_2 specific electrode.

From these results it could be concluded that the Ir film was deposited at 300 °C, total pressure of 12 Torr and O_2/(MeCp)Ir(COD) molar ratio of 125 is suitable to be used as the protective layer for specific electrode.

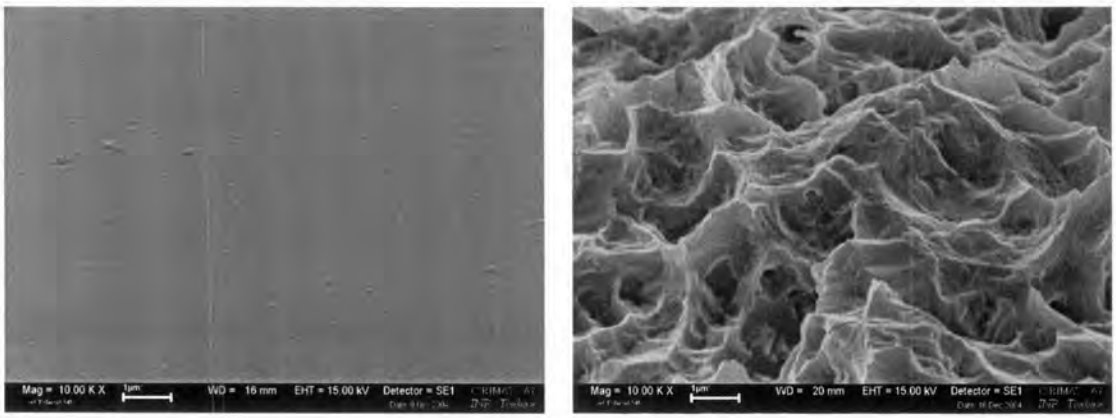

Figure 4-12 Scanning electron micrographs of Ir film a) Ir film over Si wafer and b) Ir film over 1 hr hot-HCl treated Ti substrate

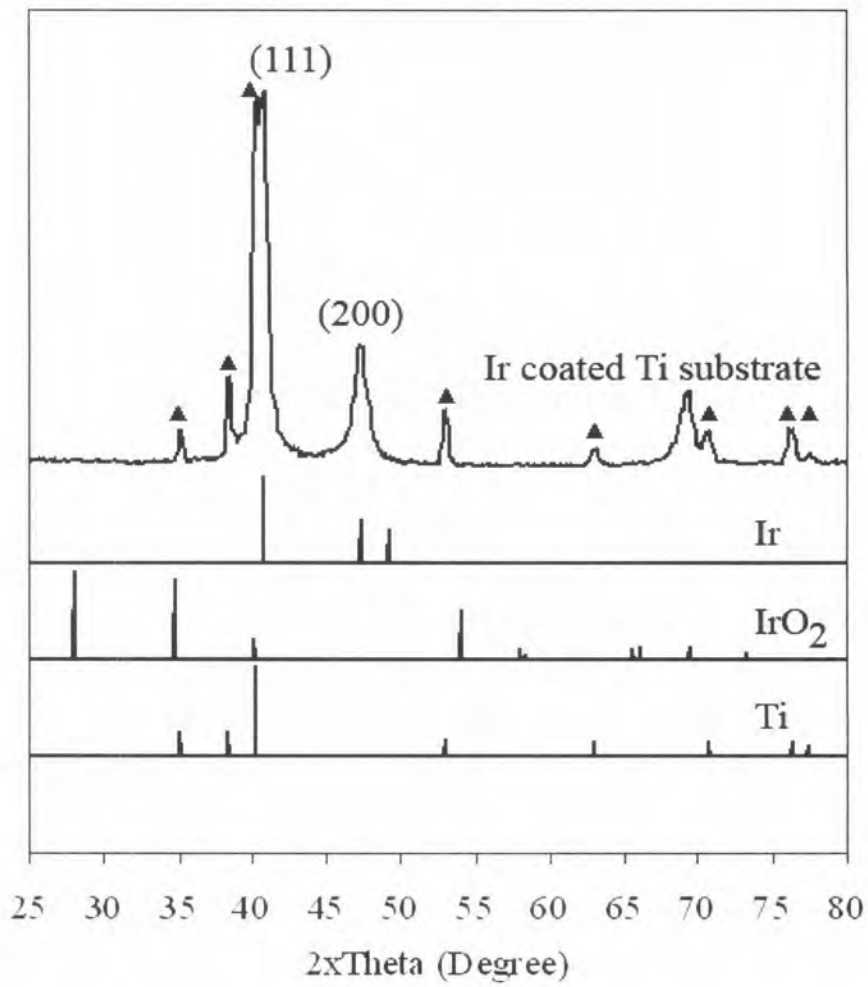

Figure 4-13 X-Ray diffraction of Ir coated Ti substrate (▲) substrate

4.1.6 Deposition of SnO_2 by MOCVD

Figure 4-14 presents the effect of feed vapor composition on the SnO_2 deposition, it was found that the increasing O_2/TET molar ratio from 300 to 1,200, the both growth rates of SnO_2 film were quite similar in first 10 cm from the entrance of the reactor. However, in isothermal zone (after first 10 cm), the O_2/TET molar ratio of 300 represented the higher growth rate of SnO_2 film. It may caused by the first 10 cm, the system temperature was still low and the internal energy of TET precursor was not enough to react with mixed oxygen. However, after system reached to the isothermal zone (after first 10 cm), the effect of TET precursor in feed vapor was outstanding. The growth rate of SnO_2 film was a function of TET concentration in feed gas composition. Similar result was found in deposition of Ir film by MOCVD in previous reports [35]. The comparison of SnO_2 film thickness at each point in the reactor was presented in Figure 4-15.

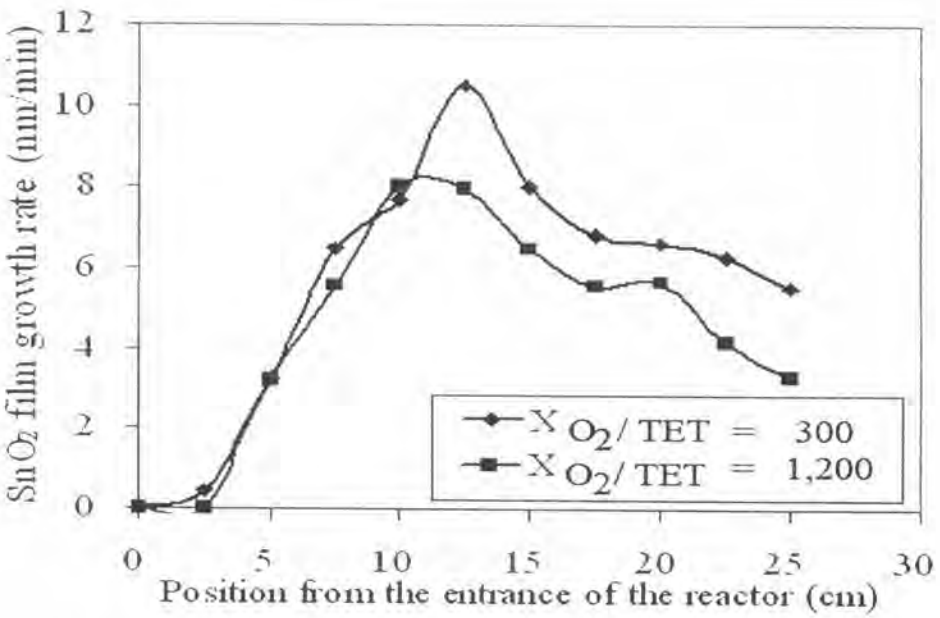

Figure 4-14 Effect of feed gas composition on SnO_2 film growth rate at 380 °C and 15 Torr

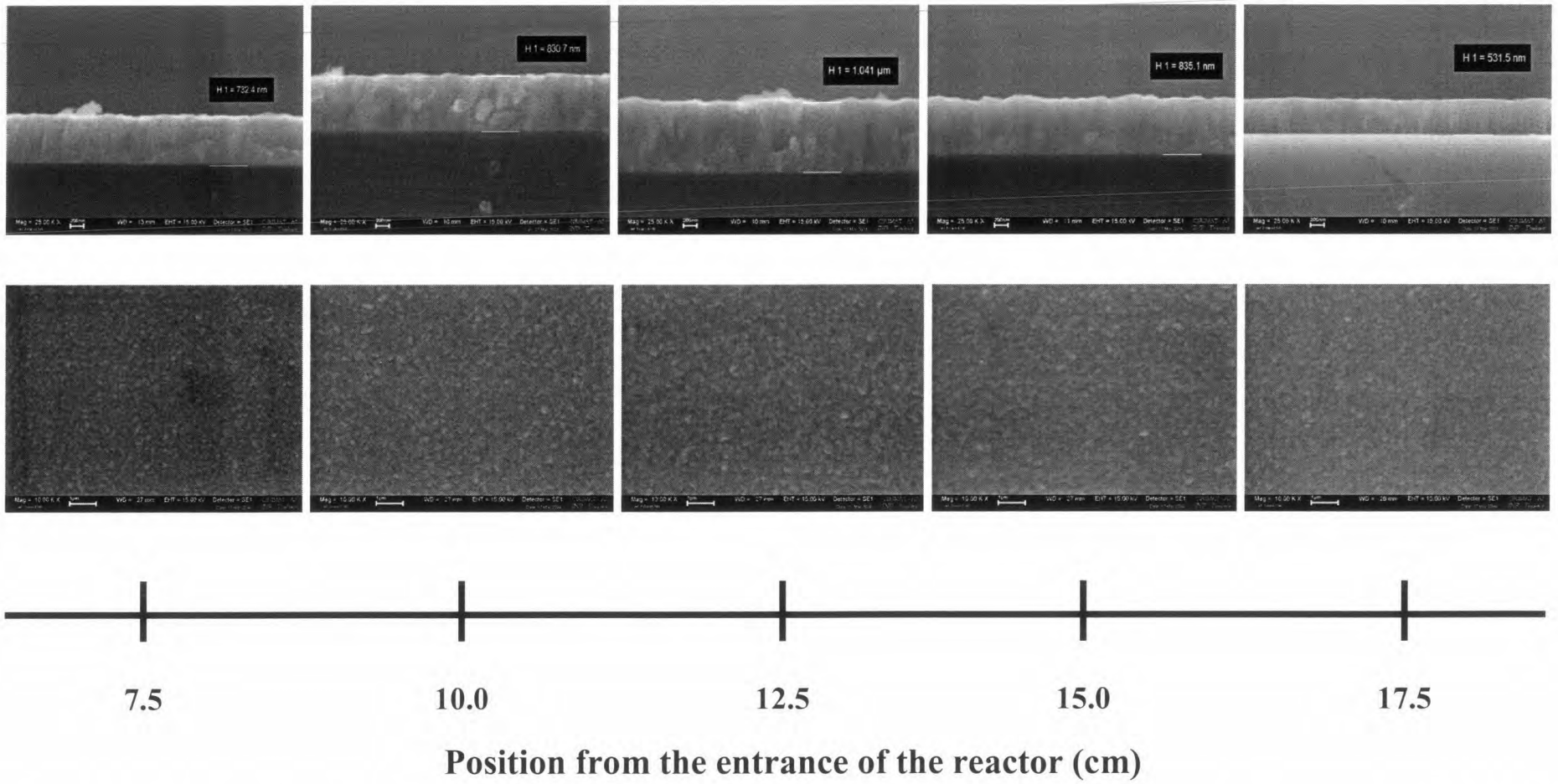

Figure 4-15 The comparison of SnO_2 film thickness at each point in the reactor, when deposition temperature of 380 °C, deposition pressure of 15 Torr and O_2/TET molar ratio of 1,200

The XRD spectra in Figure 4-16 presents that the increasing TET concentration in feed gas mixture has no influence on the microstructure of SnO_2 film. The SnO_2 film has nearly similar XRD spectra in both 300 and 1,200.

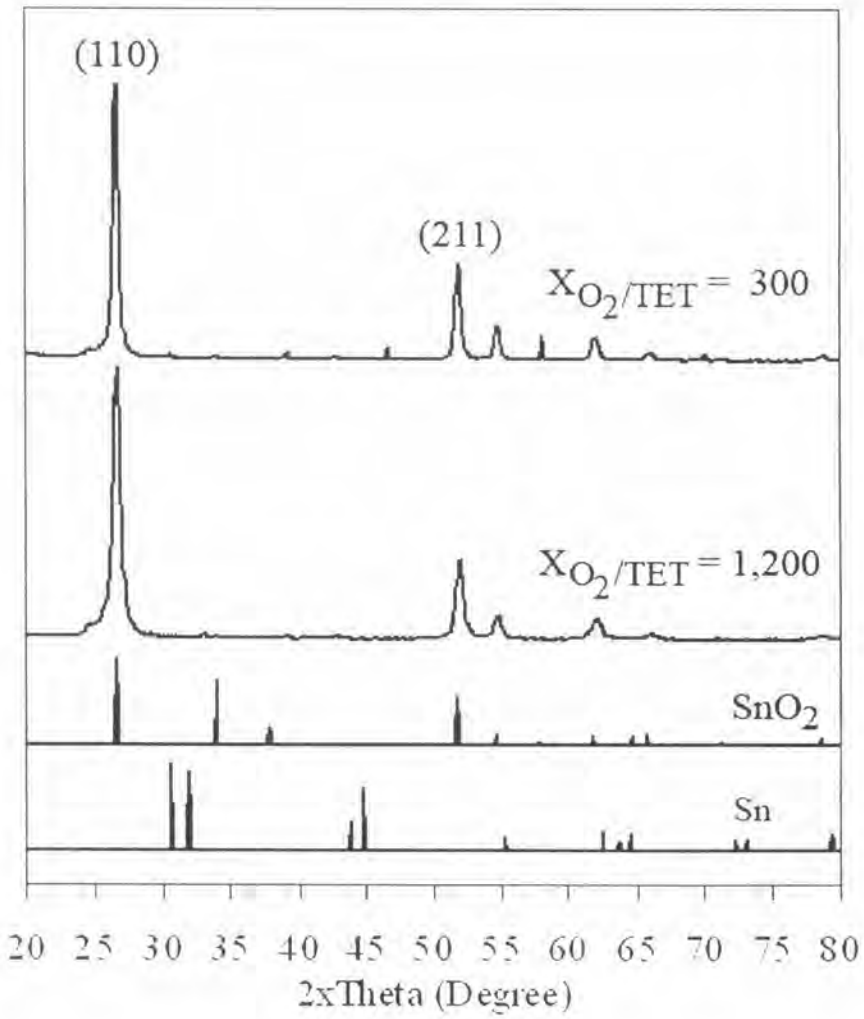

Figure 4-16 X-Ray diffraction of SnO_2 film over Si wafer at 380 °C and 15 Torr

Reaction mechanism

The reaction mechanism of SnO_2 deposition by MOCVD with using TET as precursor could be separated in homogeneous gas phase reaction and heterogeneous reaction. The mechanism was presented by Bertrand, N. [56].

The reaction mechanism was initiated by a pyrolysis of the TET that takes place at 380 °C and led to a rupture of a connection C-Sn. This homolytic rupture of a connection leads to the formation of two free radicals from both side of the TET molecule as presented in equation (4-1).

$$(CH_3\text{-}CH_2)_4Sn \rightarrow (CH_3\text{-}CH_2)_3Sn^{\bullet} + CH_3\text{-}CH_2^{\bullet} \quad (4\text{-}1)$$

Then, the triethyltin radicals ($(CH_3\text{-}CH_2)_3Sn^{\bullet}$) will be oxidized. There are two oxidation path ways of triethyltin radicals.

Mechanism 1: The triethyltin radicals are reacted with oxygen gas to produce $(CH_3\text{-}CH_2)_2Sn{=}O$ and $CH_3\text{-}CH_2O^{\bullet}$ radicals represents in equation (4-2).

$$(CH_3\text{-}CH_2)_3Sn^{\bullet} + O_2 \rightleftarrows (CH_3\text{-}CH_2)_2Sn{=}O + (CH_3\text{-}CH_2)\text{-}O^{\bullet} \quad (4\text{-}2)$$

Mechanism 2: The triethyltin radicals are reacted with oxygen gas to produce $(CH_3\text{-}CH_2)Sn^{\bullet}(OH)_2$ radicals and C_4H_8 as shown in equation (4-3).

$$(CH_3\text{-}CH_2)_3Sn^{\bullet} + O_2 \rightleftarrows (CH_3\text{-}CH_2)Sn^{\bullet}(OH)_2 + C_4H_8 \quad (4\text{-}3)$$

The $(CH_3\text{-}CH_2)_2Sn{=}O$ species, formed during the oxidation of the $(CH_3\text{-}CH_2)_3Sn^{\bullet}$ radical according to path 1, is a very active species due to its double bond in Sn=O connection. This species strongly reacts with the $CH_3\text{-}CH_2^{\bullet}$ radical to produce $(CH_3\text{-}CH_2)_2Sn\,{}^{\bullet}OH$, as shown in equation (4-4).

$$(CH_3\text{-}CH_2)_2Sn{=}O + CH_3\text{-}CH_2^{\bullet} \rightleftarrows (CH_3\text{-}CH_2)_2Sn\,{}^{\bullet}OH + C_2H_4 \qquad (4\text{-}4)$$

Mechanism 3: $(CH_3\text{-}CH_2)_2Sn\,{}^{\bullet}OH$ could be oxidized in the CVD reactor to produced $(CH_3\text{-}CH_2)SnOOH$. Then $(CH_3\text{-}CH_2)SnOOH$ is reacted with $CH_3\text{-}CH_2^{\bullet}$ to produce $(CH_3\text{-}CH_2)Sn^{\bullet}(OH)_2$ and C_2H_4 presented in equation (4-5) and (4-6).

$$(CH_3\text{-}CH_2)_2Sn^{\bullet}OH + O_2 \rightleftarrows (CH_3\text{-}CH_2)SnOOH + CH_3\text{-}CH_2\text{-}O^{\bullet} \qquad (4\text{-}5)$$

$$(CH_3\text{-}CH_2)SnOOH + CH_3\text{-}CH_2^{\bullet} \rightleftarrows (CH_3\text{-}CH_2)Sn^{\bullet}(OH)_2 + C_2H_4 \qquad (4\text{-}6)$$

Mechanism 4: However, $(CH_3\text{-}CH_2)_2Sn^{\bullet}OH$ could be reacted with O_2 to produce SnO as in equation (4-7)

$$(CH_3\text{-}CH_2)_2Sn^{\bullet}OH + O_2 \rightleftarrows SnO + C_4H_8 + {}^{\bullet}OH + H_2O \qquad (4\text{-}7)$$

The $(CH_3\text{-}CH_2)Sn^{\bullet}(OH)_2$ from both equation (4-3) and (4-6) is oxidized to produce SnO_2 as presented in equation (4-8).

$$(CH_3\text{-}CH_2)Sn^{\bullet}(OH)_2 + O_2 \rightarrow SnO_2 + C_2H_4 + {}^{\bullet}OH + H_2O \qquad (4\text{-}8)$$

In addition, the TET also reacted with $^{\bullet}OH$, produced form equation (4-7) and (4-8), to produce $(CH_3\text{-}CH_2)_3Sn(OH)$ as present in equation (4-9).

$$(CH_3\text{-}CH_2)_4Sn + {}^{\bullet}OH \rightarrow (CH_3\text{-}CH_2)_3Sn(OH) + CH_3\text{-}CH_2{}^{\bullet} \quad (4\text{-}9)$$

The $(CH_3\text{-}CH_2)_3Sn(OH)$ decompose to produce $(CH_3\text{-}CH_2)_2Sn^{\bullet}OH$ as presented in equation (4-10).

$$(CH_3\text{-}CH_2)_3Sn(OH) \rightarrow (CH_3\text{-}CH_2)_2Sn^{\bullet}OH + CH_3\text{-}CH_2{}^{\bullet} \quad (4\text{-}10)$$

There are some possible reactions in the SnO_2 listed previously. However, with the thermodynamic point of view, there are 2 reaction path ways that possible occur during the deposition of SnO_2 film could be summary.

Path way 1:

$$(CH_3\text{-}CH_2)_4Sn \rightarrow (CH_3\text{-}CH_2)_3Sn^{\bullet} + CH_3\text{-}CH_2{}^{\bullet} \quad (4\text{-}1)$$

$$(CH_3\text{-}CH_2)_3Sn^{\bullet} + O_2 \rightleftarrows (CH_3\text{-}CH_2)_2Sn{=}O + (CH_3\text{-}CH_2)\text{-}O^{\bullet} \quad (4\text{-}2)$$

$$(CH_3\text{-}CH_2)_2Sn{=}O + CH_3\text{-}CH_2{}^{\bullet} \rightleftarrows (CH_3\text{-}CH_2)_2Sn^{\bullet}OH + C_2H_4 \quad (4\text{-}4)$$

$$(CH_3\text{-}CH_2)_4Sn + {}^{\bullet}OH \rightarrow (CH_3\text{-}CH_2)_3Sn(OH) + CH_3\text{-}CH_2{}^{\bullet} \quad (4\text{-}9)$$

$$(CH_3\text{-}CH_2)_3Sn(OH) \rightarrow (CH_3\text{-}CH_2)_2Sn^{\bullet}OH + CH_3\text{-}CH_2{}^{\bullet} \quad (4\text{-}10)$$

Path way 2:

$$(CH_3\text{-}CH_2)_4Sn \rightarrow (CH_3\text{-}CH_2)_3Sn^{\bullet} + CH_3\text{-}CH_2^{\bullet} \quad (4\text{-}1)$$

$$(CH_3\text{-}CH_2)_3Sn^{\bullet} + O_2 \rightleftarrows (CH_3\text{-}CH_2)Sn^{\bullet}(OH)_2 + C_4H_8 \quad (4\text{-}3)$$

$$(CH_3\text{-}CH_2)Sn^{\bullet}(OH)_2 + O_2 \rightarrow SnO_2 + C_2H_4 + {}^{\bullet}OH + H_2O \quad (4\text{-}8)$$

$$(CH_3\text{-}CH_2)_4Sn + {}^{\bullet}OH \rightarrow (CH_3\text{-}CH_2)_3Sn(OH) + CH_3\text{-}CH_2^{\bullet} \quad (4\text{-}9)$$

$$(CH_3\text{-}CH_2)_3Sn(OH) \rightarrow (CH_3\text{-}CH_2)_2Sn^{\bullet}OH + CH_3\text{-}CH_2^{\bullet} \quad (4\text{-}10)$$

$$(CH_3\text{-}CH_2)_2Sn^{\bullet}OH + O_2 \rightleftarrows SnO + C_4H_8 + {}^{\bullet}OH + H_2O \quad (4\text{-}7)$$

In heterogeneous reaction, the SnO in gas phase is reacted with O_2 and deposited on the substrate as presented in equation (4-11) and (4-12).

$$SnO_{(g)} + O_2 \rightarrow SnO_{2(s)} + 1/2\ O_2 \quad (4\text{-}11)$$

$$SnO_{2(g)} \rightarrow SnO_{2(s)} \quad (4\text{-}12)$$

Figure 4-17 shows the more uniformly deposition of SnO_2 with decreasing residence time when the TET precursor passed through the reactor faster and had shorter time to react with mixed oxygen. However, the SnO_2 growth rate and deposition yield were decreased with decreasing residence time.

From the calibration of the system by deposited SnO_2 on Si wafer, it was found that the growth rate of SnO_2 film was smooth and uniform between 17.5-22.5 cm from the entrance of the reactor. So, in the preparation of useful electrode, the substrate was placed between 17.5-

20.5 cm from the entrance and the dashed line in Figure 4-18 is represented the placement area of substrate in SnO_2 film deposition. To measure the growth rate profile and to be sure that the system was similar to the calibration, the Si wafers still placed on the other point in the reactor as in calibration

The effect of substrate on SnO_2 film growth rate was presented in Figure 4-18. In placement area of actual substrates, the growth rate of SnO_2 film was increased when substituted Si wafer with 1 min and 1 hr HF treated tantalum and it was suddenly increased after substituted by 1 hr HCl-treated titanium and Ir coated Ti substrate. It seems to be affected from the substrates substitution. However, after considered with the roughness of substrate, it was found that the increasing SnO_2 growth rate was affected by the specific area of substrate which increased from the substrate treatment.

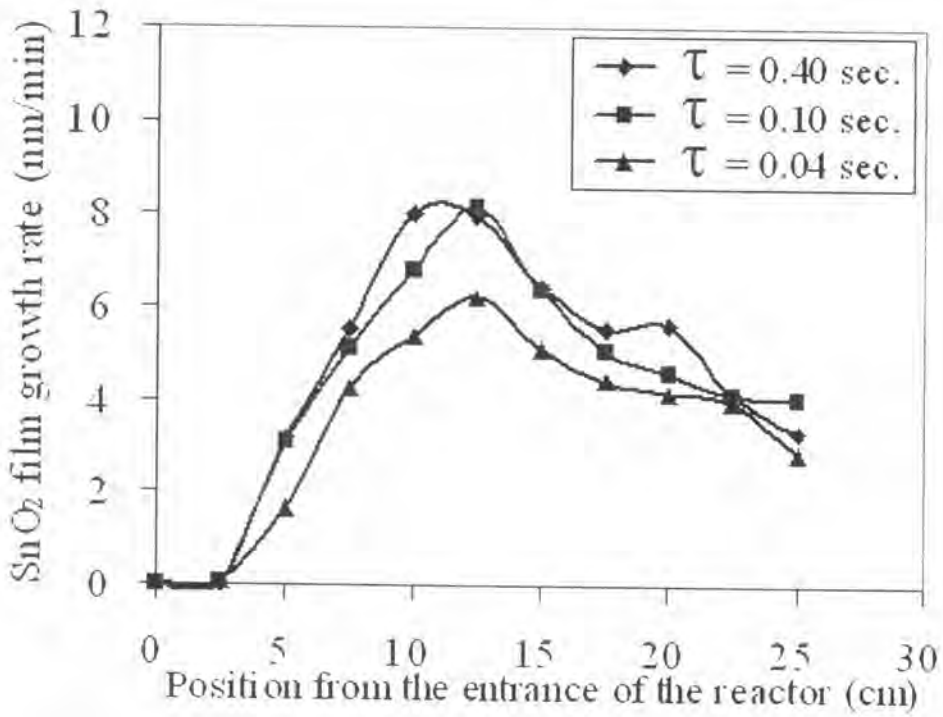

Figure 4-17 Effect of residence time on SnO_2 film growth rate at 380 °C and 15 Torr

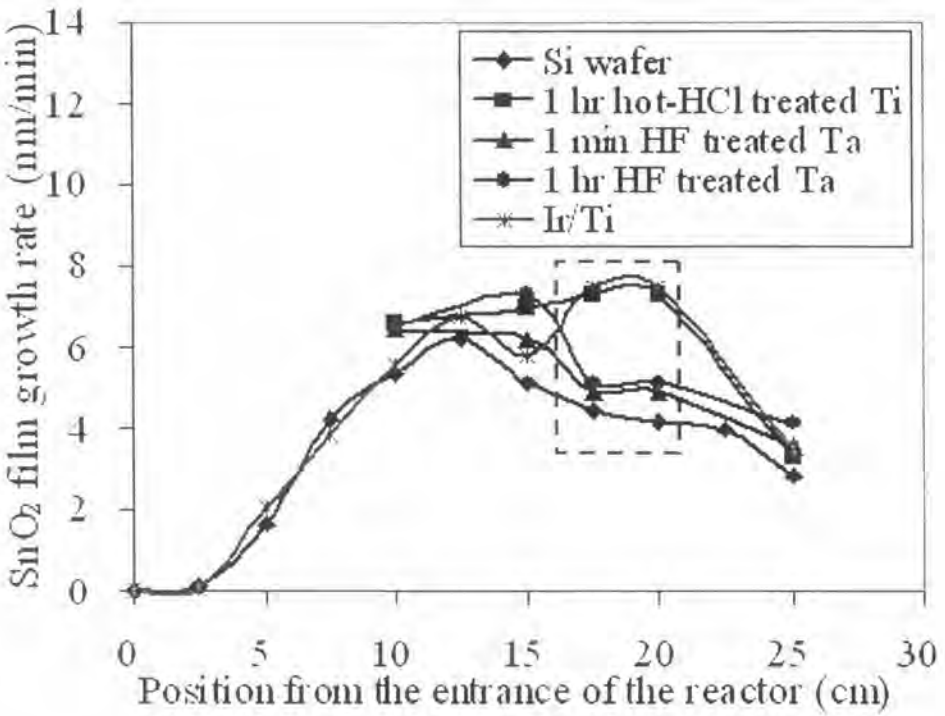

Figure 4-18 Effect of substrate on SnO_2 film growth rate at 380 °C and 15 Torr

Figure 4-19 represents the surface and cross-sectional morphology of SnO_2 film on Si wafer and Ir coated Ti substrate. The deposited SnO_2 film over Si wafer was dense, smooth and homogeneous microstructure. In case of Ir coated Ti substrate, the microstructure of SnO_2 film was still dense and homogeneous. Furthermore, it also presents the good coverage deposition on the high surface roughness of Ir coated Ti substrate.

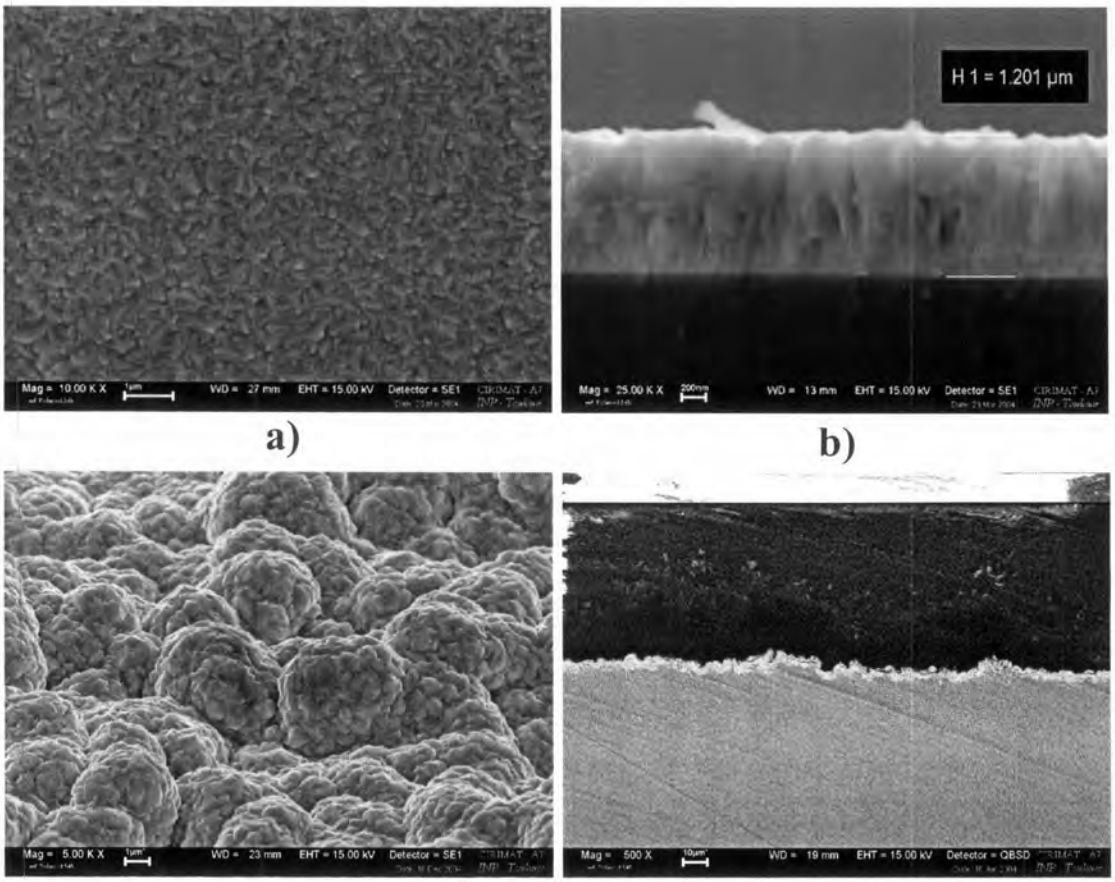

Figure 4-19 Surface and cross-sectional microstructure of SnO_2 film over various substrates a-b) Si wafer and c-d) Ir/Ti

From the results, it could be concluded that the suitable SnO_2 active coating for using as anode organic pollutant degradation was deposited at 380 ºC, 15 Torr of total pressure and 1,200 of O_2/TET molar ratio.

4.2 Activation of new electrodes

In theoretical assumption, the stoichiometric ratio between tin and oxygen is 1:2 in SnO_2. However, the non-stoichiometry of SnO_2 is presented in as prepared SnO_2 film. This initial involves a larger concentration of catalytically actives sites. The reaction takes place with the formation of adsorbed hydroxyl radicals ($^{\bullet}OH$) as presented in equation (4-13).

$$SnO_{(2-X)} + H_2O \rightarrow SnO_{(2-X)}(^{\bullet}OH) + H^+ + e^- \quad (4\text{-}13)$$

A further oxidation may take place with an increase in oxygen stoichiometry. However, at this stage the oxygen stoichiometry is still below 2, as presented in equation (4-14)

$$SnO_{(2-X)}(^{\bullet}OH)_Y \rightarrow SnO_{(2-X+Y)} + yH^+ + ye^- \quad (4\text{-}14)$$

From the decomposition of the species $SnO_{(2-x+y)}$, oxygen can be evolved with the regeneration of $SnO_{(2-x)}$ as presented in equation (4-15).

$$SnO_{(2-X+Y)} \rightarrow SnO_{(2-X)} + \frac{1}{2}yO_2 \quad (4\text{-}15)$$

Under anodic polarization between hydrogen and oxygen evolution reaction, reconstruction of the film surface occurs with loss of defectivity. The oxygen evolution reaction can be through this step as presented in equation (4-16)

$$SnO_2(^{\bullet}OH) \longrightarrow SnO_2 + \frac{1}{2}O_2 + H^+ + e^- \quad (4\text{-}16)$$

The role played by the anodic precondition could be the progressive of the y value towards x.

Figure 4-20 represents the activation of SnO_2/Ir/Ti electrode with the applied current of 38.4 mA (current density 10 mA/cm^2). The potential was increased from 0-430 min to the maximum potential due to the transfer oxygen from adsorbed hydroxyl to lattice for improving oxygen stoichiometry as equation (4-14). After the activation completed, the electrode was ready to work at the constant potential.

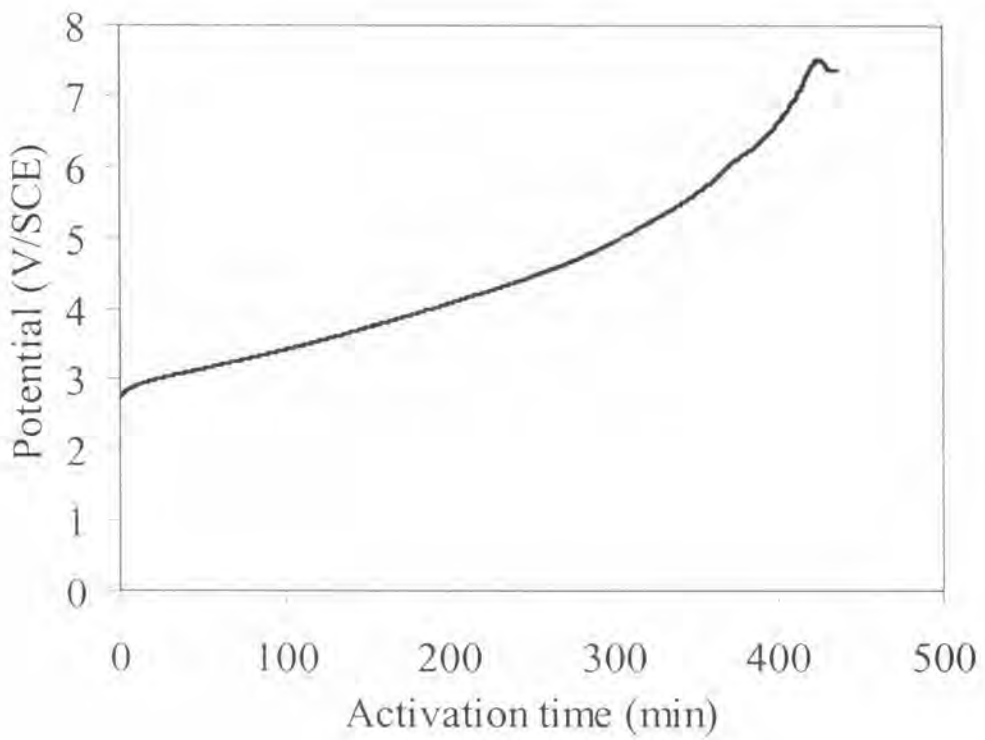

Figure 4-20 Activation of SnO_2/Ir/Ti electrode, current density of 10 mA/cm^2

Figure 4.21 represents the activation of SnO_2/TaC/Ta. The potential oscillations were observed, that could be explained by the modification of electrode surface during the transfer of oxygen to the lattice increased the internal stress of oxidized layer. Furthermore, the adhesion between SnO_2 layer and TaC was damaged by the free carbon that remained on TaC surface. Figure 4-22 presents the SnO_2/TaC/Ta after activation, the passivating SnO_2 layer was observed.

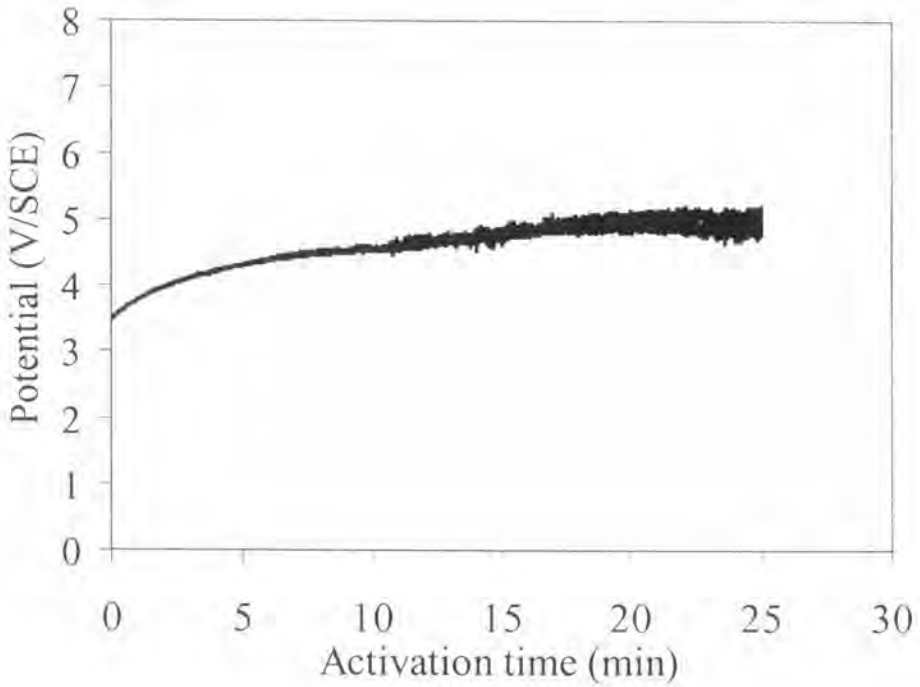

Figure 4-21 Activation of SnO_2/TaC/Ta electrode, current density of 10 mA/cm^2

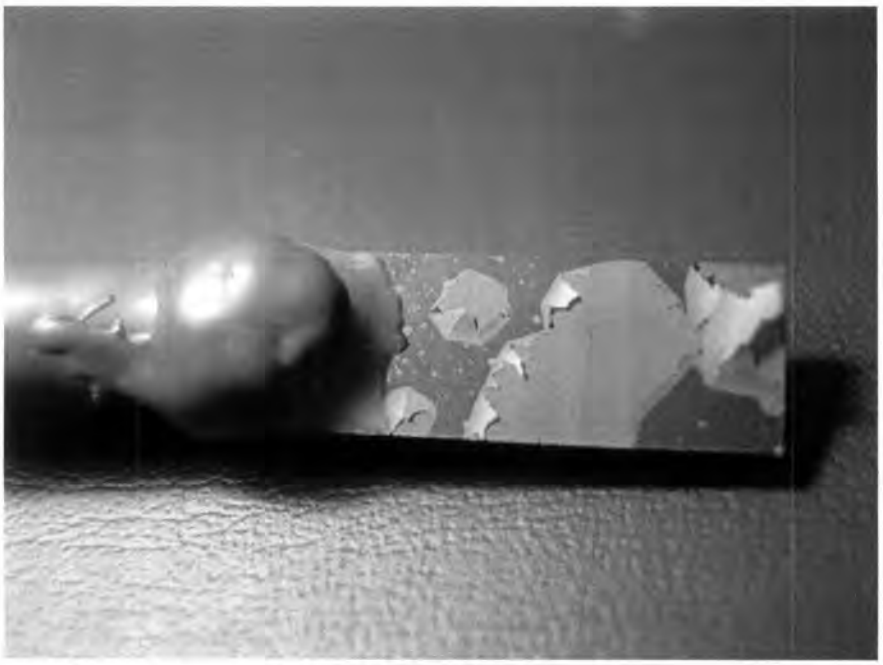

Figure 4-22 The SnO_2/TaC/Ta after chronopotentiometrical activation current density of 10 mA/cm^2

4.3 Application of SnO_2/Ir/Ti specific electrodes in batch process with model solution

It is well known that SnO_2 electrode is powerful for organic pollutant destruction by anodic oxidation [3, 15-17, 41]. Figure 4-23 represents the destruction of oxalic acid by specific SnO_2/Ir/Ti electrode with 2 different SnO_2 film thicknesses. It appears that SnO_2 thickness was not a great influence on the performance of the electrode.

The two regions of organic pollutant degradation can be defined. In first region ($t \leq 2$ hr), the TOC of model solution decreased immediately, but in the second region ($t > 2$ hr), the TOC of model solution decreased

slightly. It could be explained that the reaction mechanism was changed after first 2 hr due to the decreasing TOC concentration in model solution. The detail of reaction mechanism will be explained in the section of kinetic investigation.

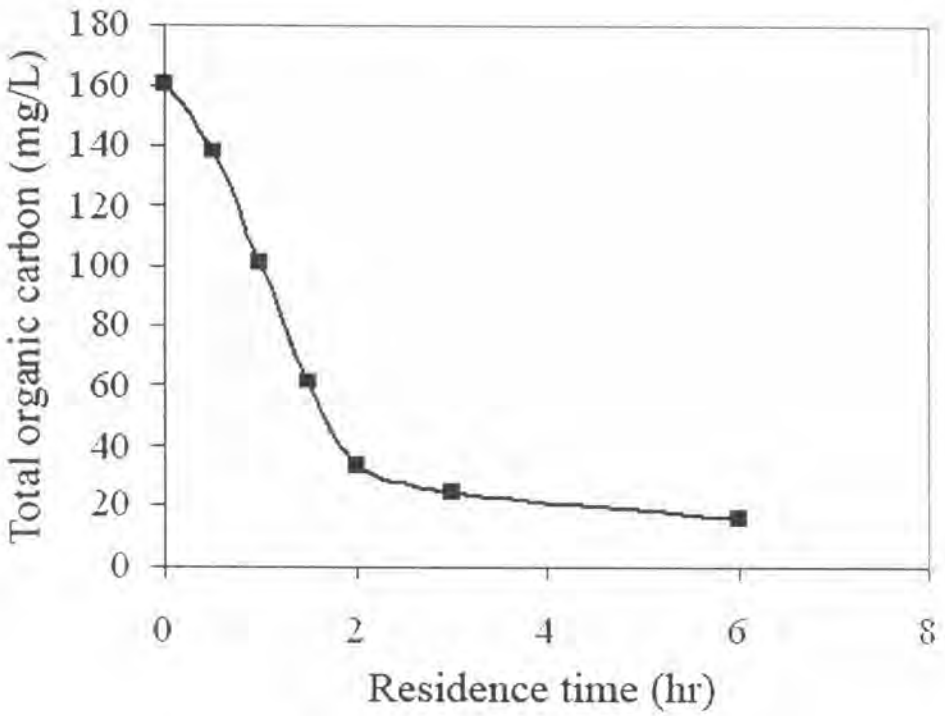

Figure 4-23 Total organic carbon degradation by using of SnO_2/Ir/Ti, electrode surface area of 3.2 cm^2 and current density of 5 mA/cm^2

4.3.1 Influence of SnO_2 active film thickness

Figures 4-24 and 4-25 represent the effect of SnO_2 film thickness on the pollutant degradation performance. The results presented that the SnO_2 thickness does not have the great effect on the oxalic acid destruction. It may be caused by the production of adsorbed hydroxyl radicals was occurred only at the surface of electrode. However,

Duverneuil et al. [41] proposed that the optimum SnO_2 thickness is 2-5 micron because microcracks have been observed for thicker SnO_2 film thickness due to the thermal stress in SnO_2 film during the deposition process.

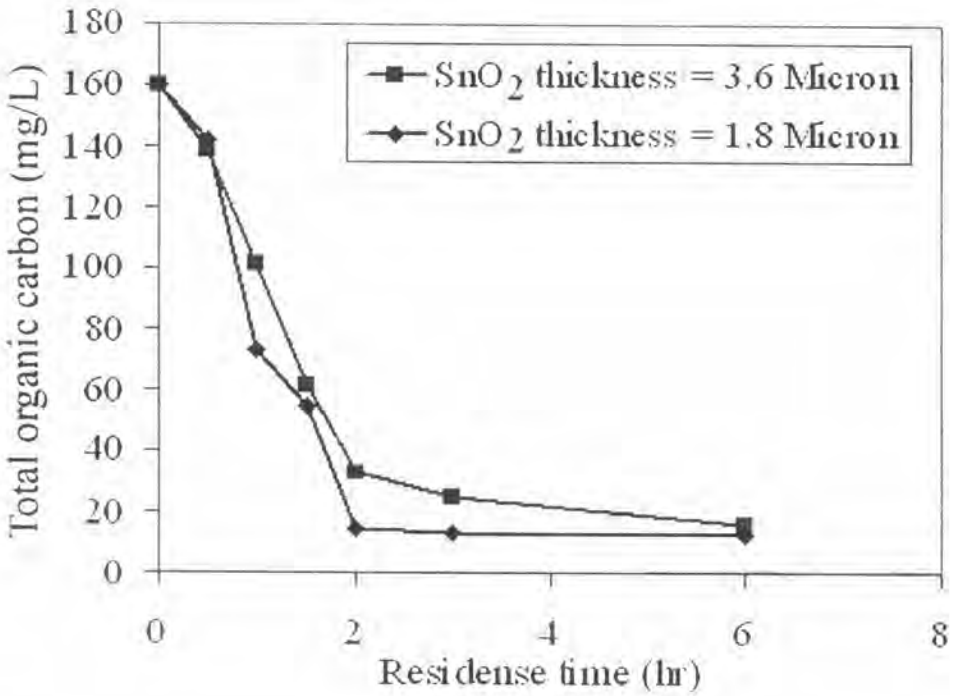

Figure 4-24 Effect of SnO_2 layer thickness on TOC removal by using of SnO_2/Ir/Ti, electrode surface area of 3.2 cm^2 and current density of 5 mA/cm^2

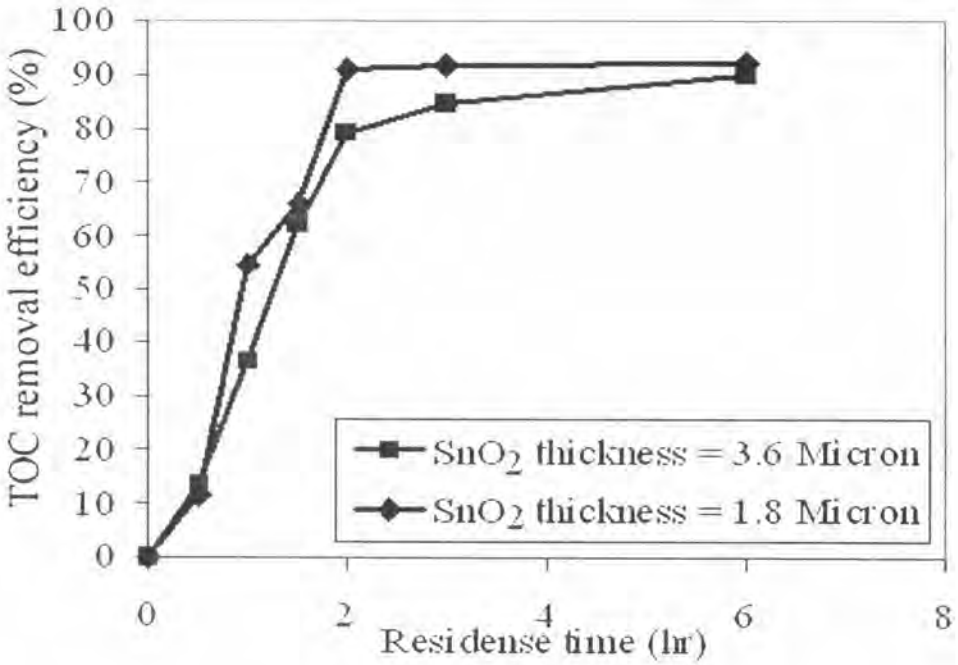

Figure 4-25 Effect of SnO_2 layer thickness on TOC removal efficiency by using of SnO_2/Ir/Ti, electrode surface area of 3.2 cm^2 and current density of 5 mA/cm^2

4.3.2 Kinetic investigation

Regarding the kinetics of TOC degradation by using oxalic acid as model solution with 160.4 mg/L initial TOC concentration, we found that the kinetic of TOC degradation occurs as a two-step process. Firstly, when the solution contains the high TOC concentration, the kinetic was the zero-order with respect to TOC of the model solution. The other one, at low TOC concentration, the kinetic was the first-order with respect to TOC concentration in the model solution.

At t ≤2 hr, the kinetics of TOC degradation was the zero-order reaction. The TOC concentration profile of the model solution was presented in Figure 4-26 and expressed by

$$TOC_t = TOC_i - k_O t \qquad (4\text{-}17)$$

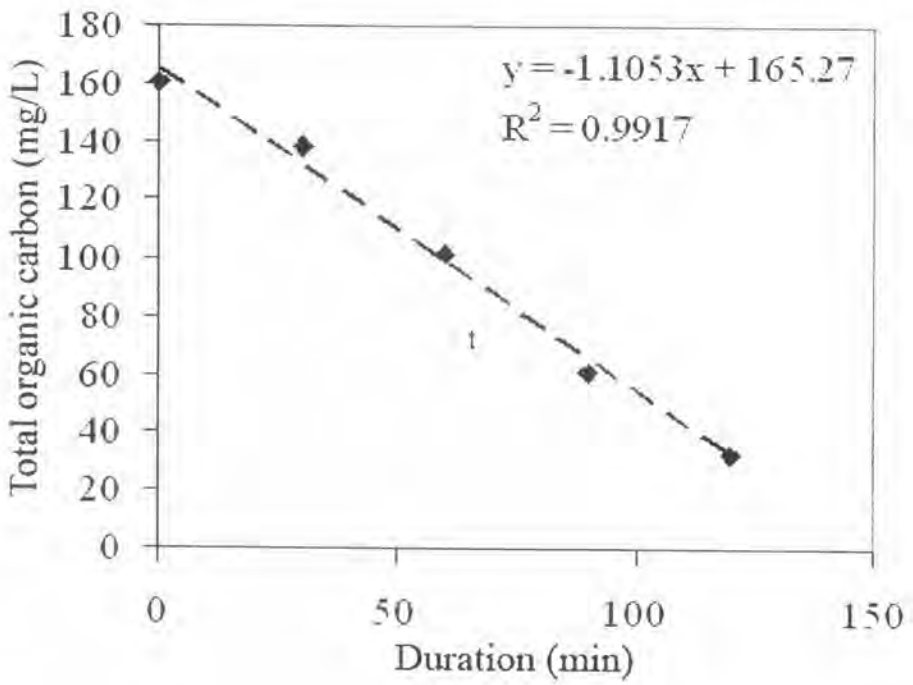

Figure 4-26 TOC concentration profile of model solution when t ≤2 hr by using of SnO_2/Ir/Ti, SnO_2 thickness of 1.8 micron, electrode surface area of 3.2 cm^2 and current density of 5 mA/cm^2

At t > 2 hr, the kinetics of TOC degradation was the first-order reaction. The TOC concentration profile of the model solution was presented in Figure 4-27 and expressed by

$$TOC_t = TOC_i \cdot \exp\left[-k_1(t - t^*)\right] \qquad (4\text{-}18)$$

Where

TOC_i	initial TOC concentration of model solution (mg/L)
TOC_t	TOC concentration of model solution at time t (mg/L)
TOC_{t^*}	TOC concentration of model solution at transition time t* (mg/L)
t	residence time (min)
t^*	transition time (min), in this case was 120 min
k_0	rate constant for the zero-order reaction (mg/L-min)
k_1	rate constant for first-order reaction (min^{-1})

In this case, we found that the average k_0 = 1.1855 mg/L-min and $k_1 = 0.0017\ min^{-1}$.

Figure 4-28 presents the comparison of experimental data and developed kinetic model. The developed kinetic model shows the good fit with the experimental data.

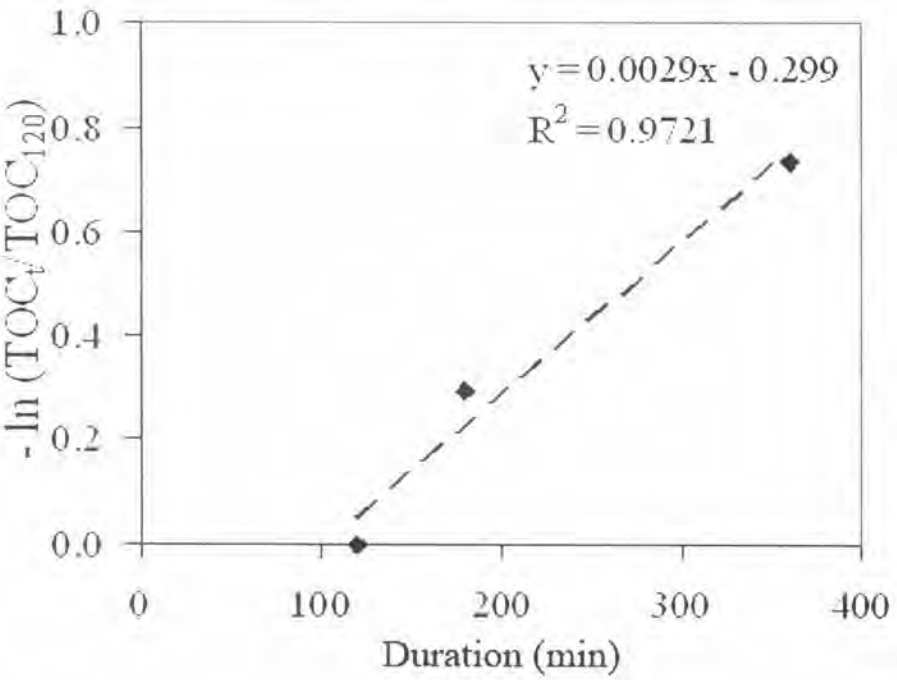

Figure 4-27 TOC concentration profile of model solution when t > 2 hr by using of SnO_2/Ir/Ti, SnO_2 thickness of 1.8 micron, electrode surface area of 3.2 cm^2 and current density of 5 mA/cm^2

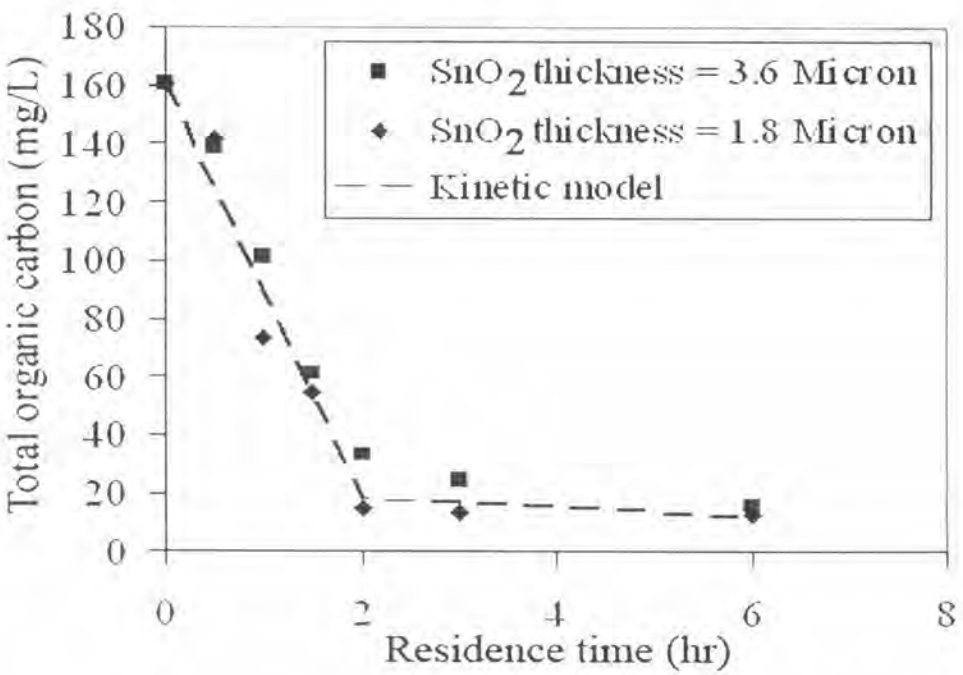

Figure 4-28 Comparison of experimental data and kinetic model (data from Figure 4-24)

4.3.3 Influence of current density

Figure 4-29 shows the influence of current density. The increasing current density from 5 to 10 mA/cm^2, leads to less degradation rate of oxalic acid by electrochemical oxidation. When the effect of charge loading to the system was considered in Figure 4-30, the system presents the higher charges required for destruction the same amount of oxalic acid. The system at current density at 5 mA/cm^2 has oxalic acid degradation in term of TOC removal efficiency twice greater than that at 10 mA/cm^2.

This behavior is the characteristic of diffusion-controlled processes [54]. In such system, the increasing of current density cannot increase the organic removal efficiency at the electrode, but only favors oxygen evolution as the anodic side reaction. When the system does not generate only adsorbed hydroxyl radicals or other active oxygen, the decreasing of organic pollutant removal efficiency was observed.

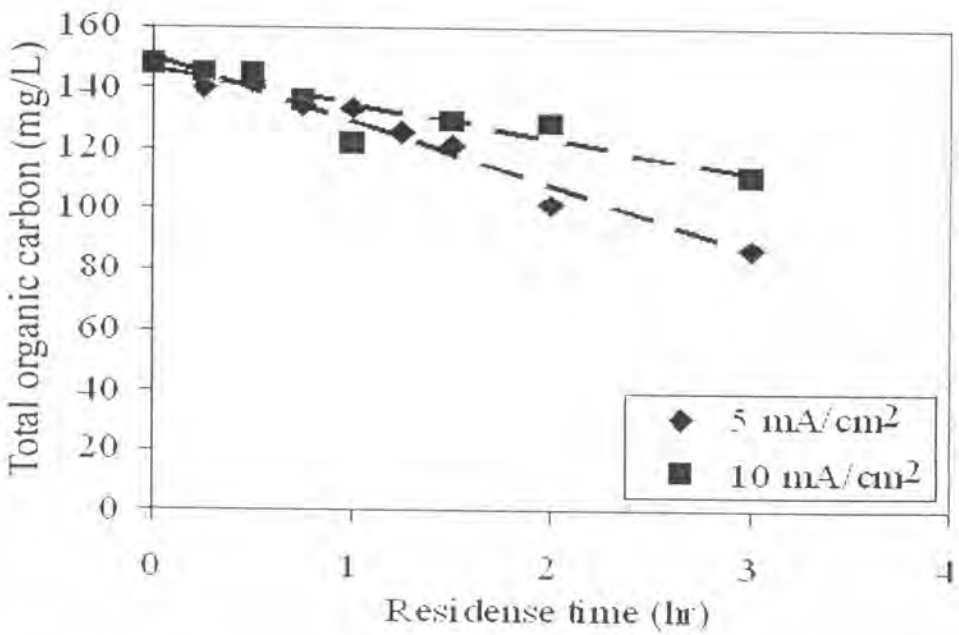

Figure 4-29 Effect of current density on TOC removal by using of SnO_2/Ir/Ti, SnO_2 thickness of 1.8 micron and electrode surface area of 3.2 cm^2

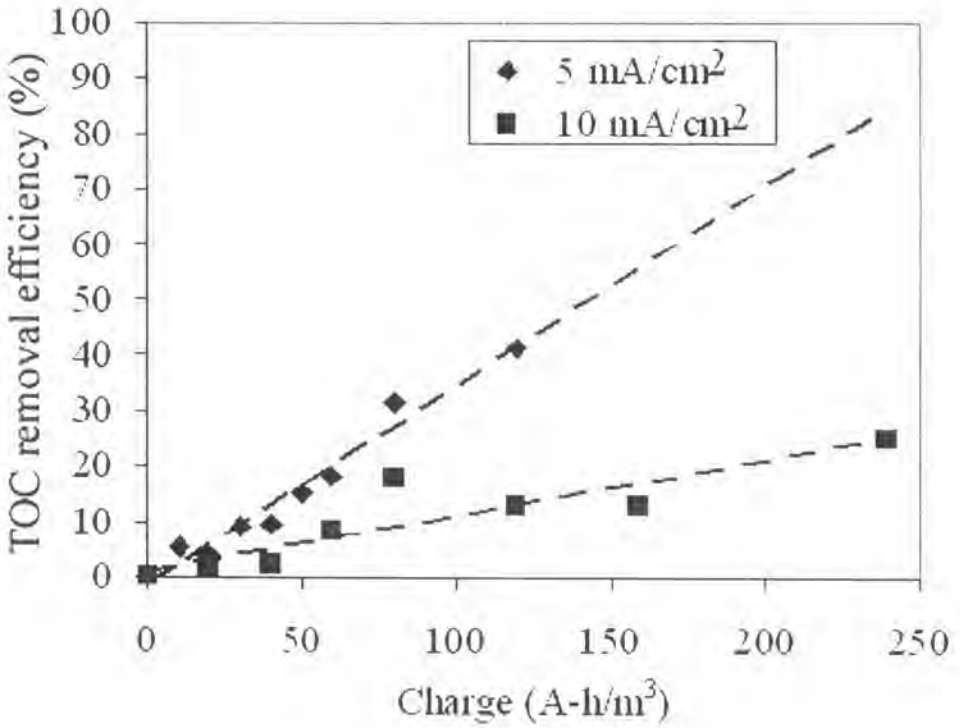

Figure 4-30 Effect of charge loading to the system on TOC removal by using of SnO_2/Ir/Ti, SnO_2 thickness of 1.8 micron and electrode surface area of 3.2 cm^2

Although, Ta and TaC/Ta substrates have some attractive properties to be used as substrate for specific SnO_2 electrode, but Ta substrate was brittle and lose some physical properties after etched by HF. In case of SnO_2/TaC/Ta, the passivation of SnO_2 film was observed after a few minutes in electrochemical characterization that affected by some free carbon between SnO_2 film and TaC surface.

4.4 Application of SnO_2/Ir/Ti specific electrodes for actual restaurant wastewater

4.4.1 Characterization of restaurant wastewater

Although, the wastewater from Chulalongkorn University Student Canteen had been treated by the physical treatment process as grease trap, but it still had high organic strength. Table 4-1 presents the characterization of effluent from Chulalongkorn University Student Canteen. It shows that the effluent has high BOD, COD and oil and grease, which cause the big problem for public wastewater collection and treatment system.

Table 4-1 Characterization of wastewater from Chulalongkorn University Student Canteen

Parameter	Value
pH	4.62
BOD (mg/L)	1,050
COD (mg/L)	2,000
TOC (mg/L)	896
Oil and Grease (mg/L)	2,270

The experiments in continuous mixed flow reactor were carried out for the determination of the effects of the current density, residence time and SnO_2 film thickness on organic pollutant degradation. Due to the very small electrode area and easy to observe the change of TOC, the wastewater that feed to the system was diluted to around 140 mg TOC/L. The current density was 5 and 10 mA/cm^2 and the residence time was 2 and 3 hr.

4.4.2 Influence of current density

The influence of current density in continuous mixed flow experiments is presented in Figure 4-31. The electrochemical degradation of organic pollutants presented in actual restaurant wastewater takes place slowly and its TOC removal efficiency presented in Figure 4-32 is higher at lower current density. The gain in efficiency being overwhelmed by the lower current values applied. This result may not be surprising on the basis of the previously discussed influence of current density in batch experiments, which indicated to a weak behavior for the characteristic of diffusion-controlled processes. Increase in current density cannot increase the organic removal efficiency at the electrode, but only favours the anodic side reaction which decreased the organic pollutant removal efficiency. It agrees with Figures 4-33 and 4-34 that the destruction of organic pollutants in term of COD was decreased with increasing of the current density from 5 to 10 mA/cm^2.

The equilibrium efficiencies of both TOC and COD removal were 62% when current density was 5 mA/cm^2. While their removal efficiencies were 47% when the current density was 10 mA/cm^2.

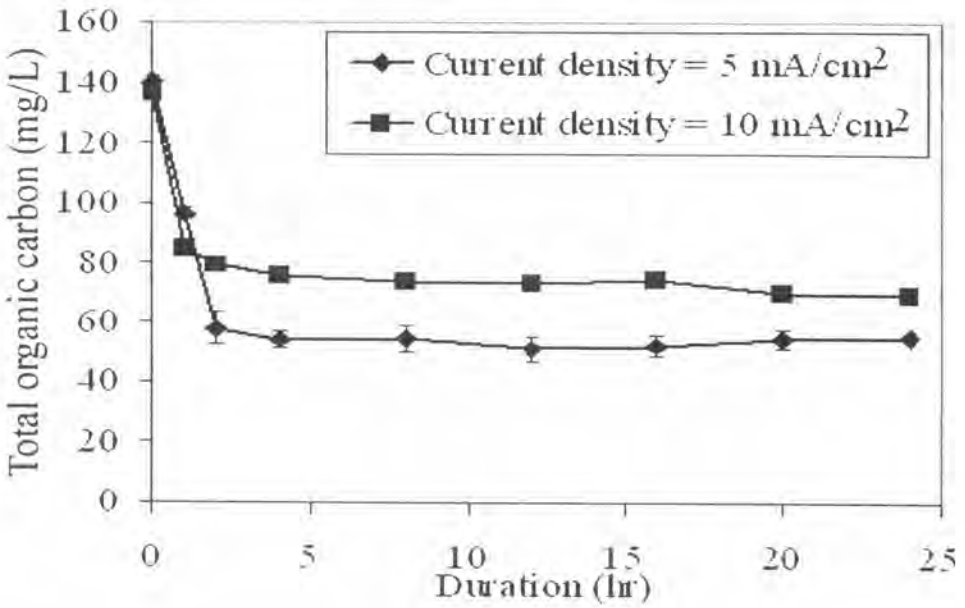

Figure 4-31 Effect of current density on TOC removal in continuous restaurant wastewater treatment by using of SnO_2/Ir/Ti, SnO_2 thickness of 1.8 micron and electrode surface area of 3.2 cm^2

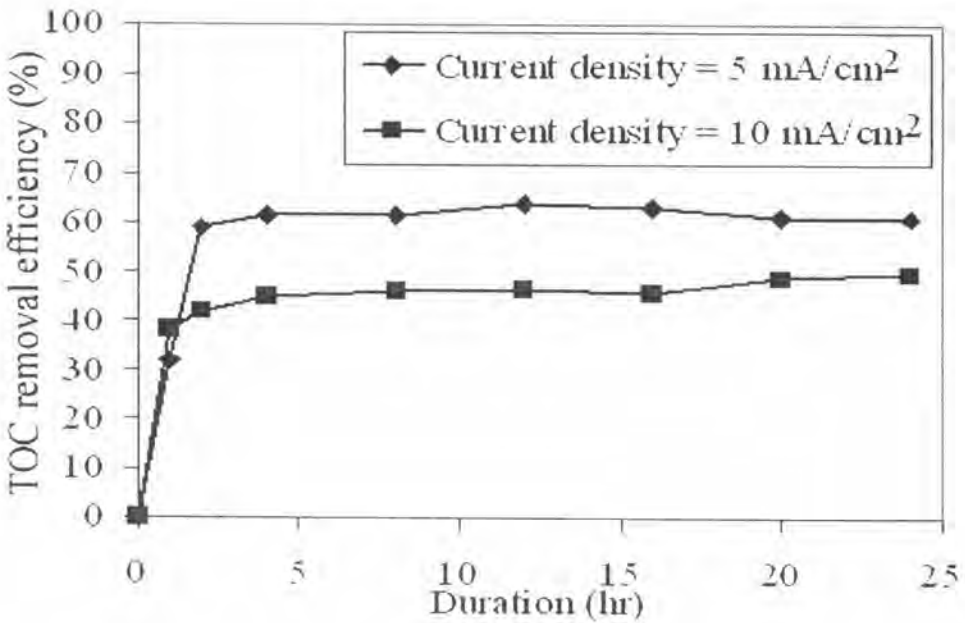

Figure 4-32 Effect of current density on TOC removal efficiency in continuous restaurant wastewater treatment by using of SnO_2/Ir/Ti, SnO_2 thickness of 1.8 micron and electrode surface area of 3.2 cm^2

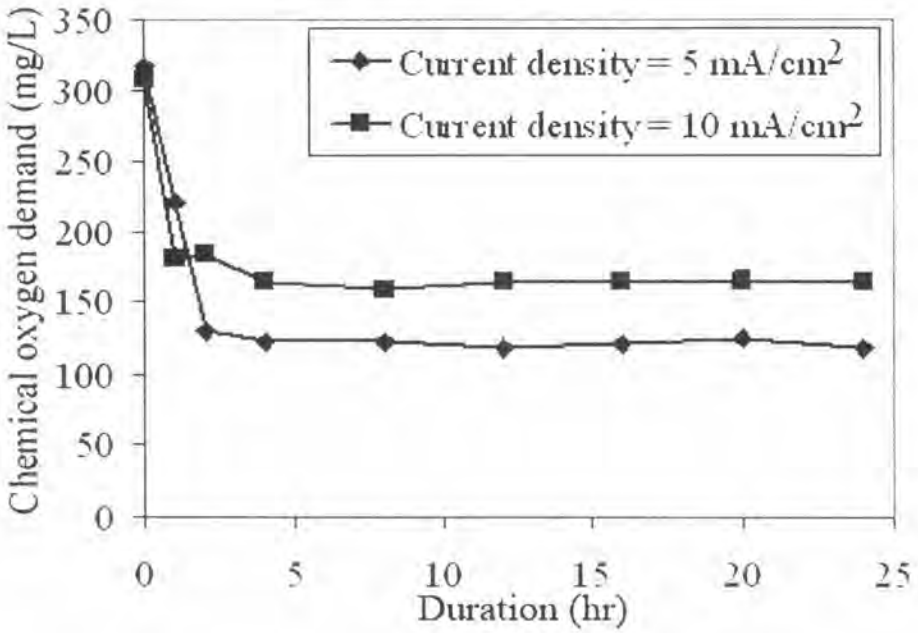

Figure 4-33 Effect of current density on COD removal in continuous restaurant wastewater treatment by using of SnO_2/Ir/Ti, SnO_2 thickness of 1.8 micron and electrode surface area of 3.2 cm^2

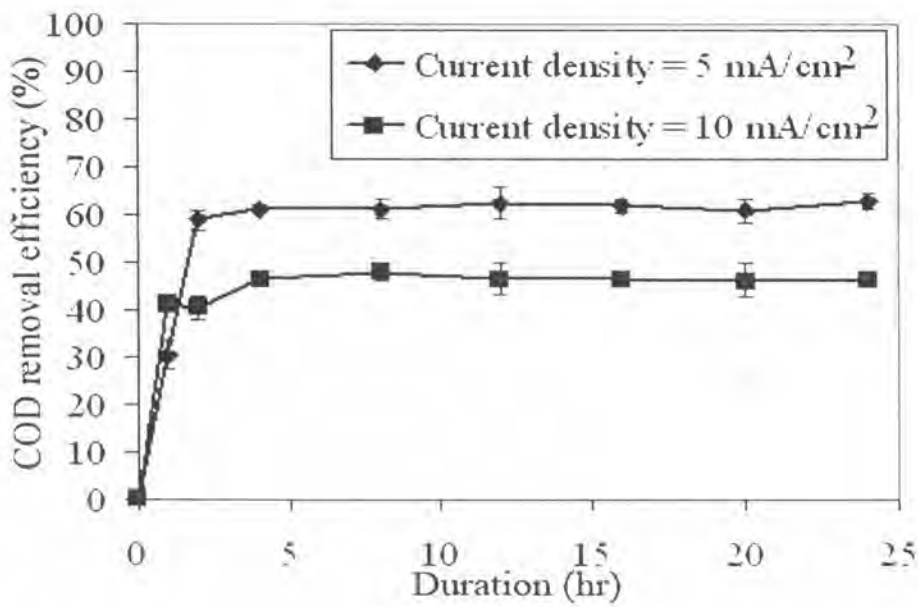

Figure 4-34 Effect of current density on COD removal efficiency in continuous restaurant wastewater treatment by using of SnO_2/Ir/Ti, SnO_2 thickness of 1.8 micron and electrode surface area of 3.2 cm^2

4.4.3 Influence of residence time

Although the results in batch experiments represented that the increasing of residence time after first 2 hr was not greatly affect on the organic pollutant degradation efficiency due to the change reaction order from zero-order to first-order reaction with reduction of TOC. However, it would be practical interest to test how much an increase or decrease in the wastewater flow rate affects the TOC removal of the restaurant wastewater. This is demonstrated in Figures 4-35 and 4-36. Because of fixed total volume of the continuous mixed flow reactor at 18 ml, an increase in the wastewater flow rate from 0.10 to 0.15 ml/min translates to a proportional decrease in the wastewater hydraulic residence time from 3 to 2 hr.

Normally, a reduction in residence time would expectedly lead to a decrease in the wastewater TOC removal. But, in this case, increasing of residence time does not proportionally increase TOC removal. As seen in Figures 4-35 and 4-36, the TOC removal increases from around 55 to 62 % with the increase in the residence time from 2 to 3 hr. These results were also observed in the removal of COD and represented in Figures 4-37 and 4-38. The COD removal increased from around 54 to 62 % with the increase in residence time from 2 to 3 hr.

It could be explained by the increasing of residence time from 2 to 3 hr has not strongly affected on the TOC and COD removal due to the fast reaction with zero-order reaction occurred in the first 2 hr. Then, the reaction was changed to the slower step with the first-order reaction as we found in the batch experiments.

Hence, it would be more economical to operate the electrochemical treatment at a lower residence time as long as the pollutant concentration of the treated wastewater meets the safe discharge requirement.

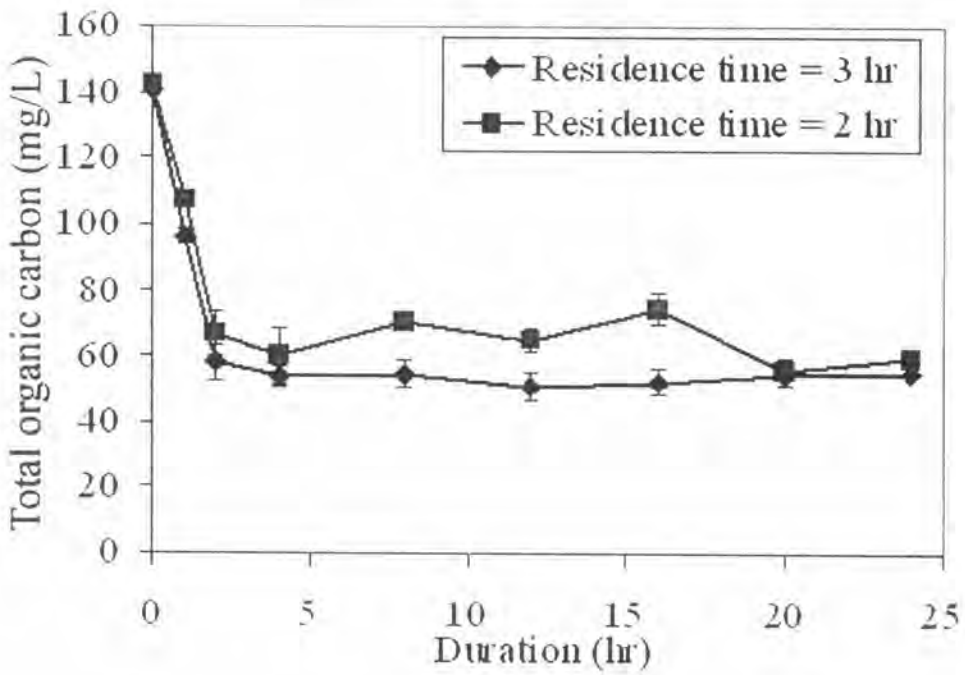

Figure 4-35 Effect of residence time on TOC removal in continuous restaurant wastewater treatment by using of SnO_2/Ir/Ti, SnO_2 thickness of 1.8 micron, current density 5 mA/cm^2 and electrode surface area of 3.2 cm^2

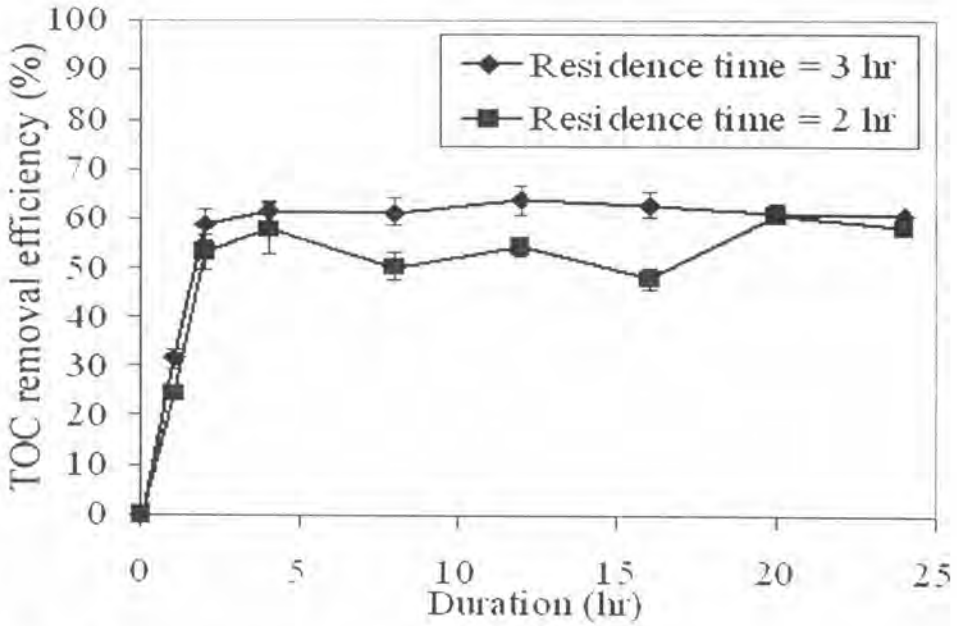

Figure 4-36 Effect of residence time on TOC removal efficiency in continuous restaurant wastewater treatment by using of SnO_2/Ir/Ti, SnO_2 thickness of 1.8 micron, current density 5 mA/cm^2 and electrode surface area of 3.2 cm^2

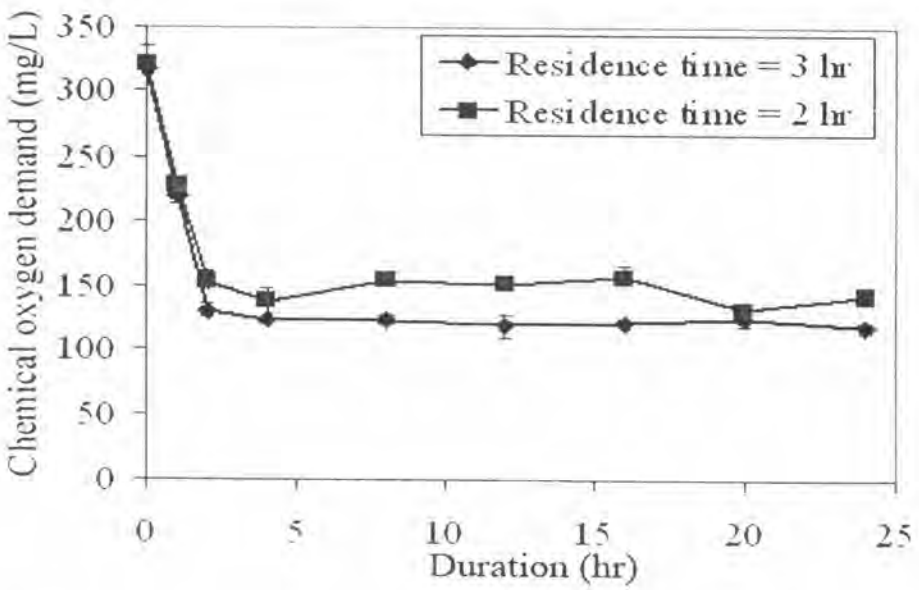

Figure 4-37 Effect of residence time on COD removal in continuous restaurant wastewater treatment by using of SnO_2/Ir/Ti, SnO_2 thickness of 1.8 micron, current density of 5 mA/cm^2 and electrode surface area of 3.2 cm^2

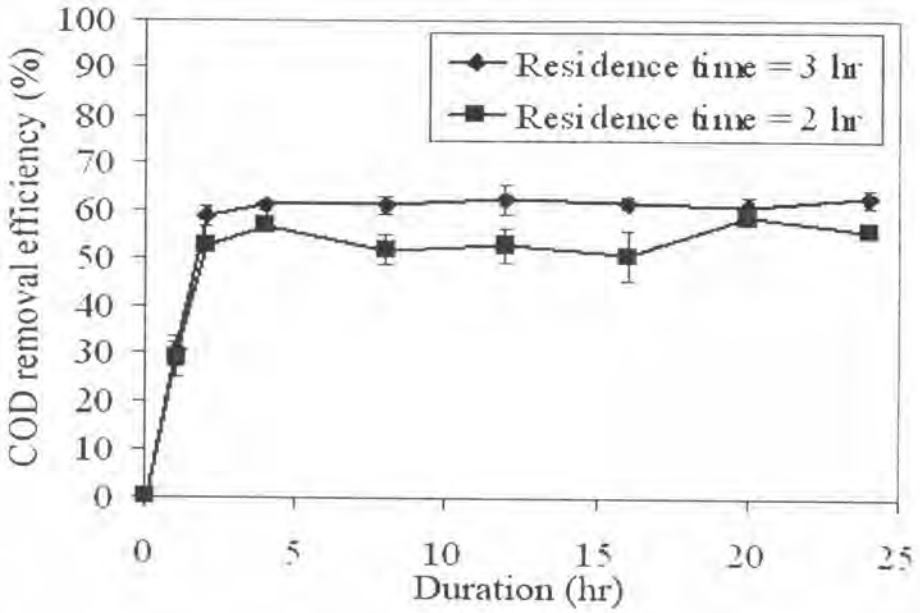

Figure 4-38 Effect of residence time on COD removal efficiency in continuous restaurant wastewater treatment by using of SnO_2/Ir/Ti, SnO_2 thickness of 1.8 micron, current density of 5 mA/cm^2 and electrode surface area of 3.2 cm^2

4.4.4 Influence of SnO_2 active layer thickness

Figures 4-39 and 4-40 represents the effect of SnO_2 film thickness on the TOC degradation performance in continuous electrochemical oxidation. Similar to the pollutant degradation of organic pollutant in batch experiment, it shows that the SnO_2 active layer thickness was not a great influence on the TOC removal efficiency because the adsorbed hydroxyl radicals for organic pollutant degradation were produced only at the surface of electrode. However, the TOC removal efficiency was around 62% with the 1.8 micron of SnO_2 active layer while the efficiency was reduced to 51% with the SnO_2 active layer thickness of 3.6 micron. It agrees with the removal of COD from restaurant wastewater as presented

in Figure 4-41 and 4-42. The COD removal efficiency was 62% when the thickness of SnO_2 active layer was 1.8 micron. However, the efficiency was decreased to 50% when the thickness of SnO_2 active layer was 3.6 micron.

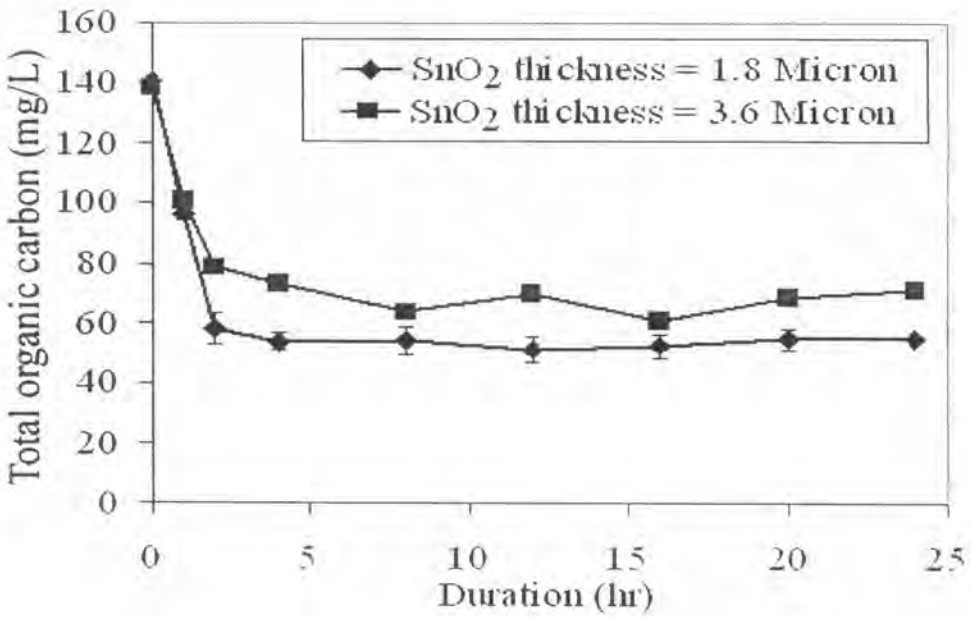

Figure 4-39 Effect of SnO_2 layer thickness on TOC removal in continuous restaurant wastewater treatment by using of SnO_2/Ir/Ti, current density of 5 mA/cm^2 and electrode surface area of 3.2 cm^2

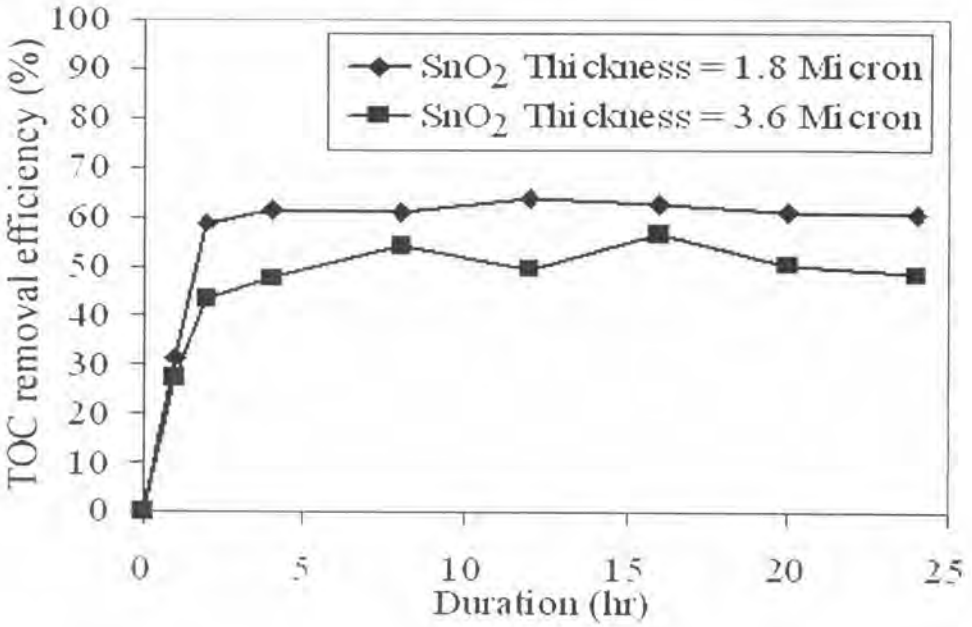

Figure 4-40 Effect of SnO_2 layer thickness on TOC removal efficiency in continuous restaurant wastewater treatment by using of SnO_2/Ir/Ti, current density of 5 mA/cm^2 and electrode surface area of 3.2 cm^2

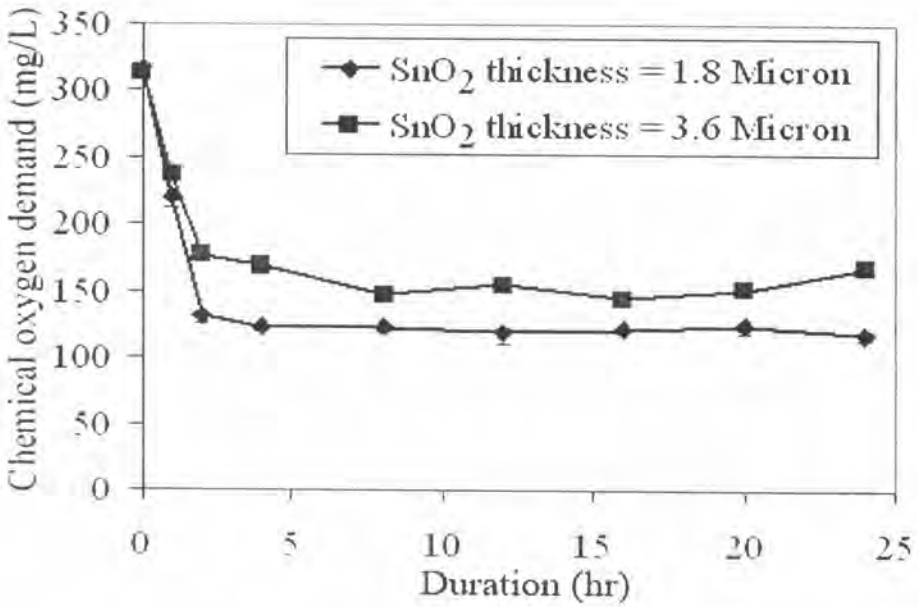

Figure 4-41 Effect of SnO_2 layer thickness on COD removal in continuous restaurant wastewater treatment by using of SnO_2/Ir/Ti, current density 5 mA/cm^2 and electrode surface area 3.2 cm^2

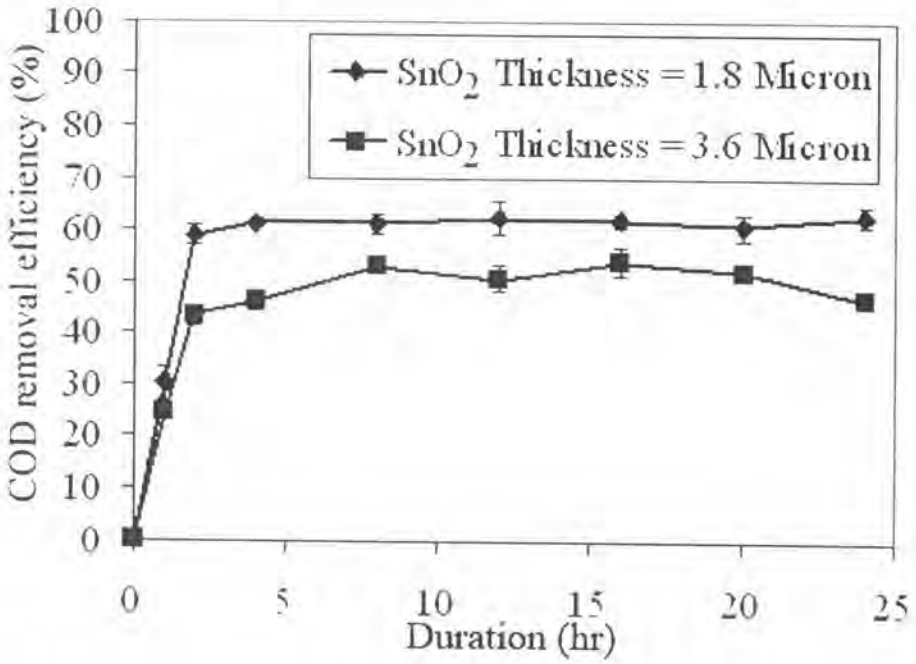

Figure 4-42 Effect of SnO_2 layer thickness on COD removal efficiency in continuous restaurant wastewater treatment by using of SnO_2/Ir/Ti, current density of 5 mA/cm^2 and electrode surface area of 3.2 cm^2

4.5 Treatment cost analysis of restaurant wastewater treatment by electrochemical oxidation

The cost analysis of restaurant wastewater treatment by electrochemical oxidation is presented in Tables 4-2, 4-3 and 4-4. The operating cost was calculated based on the adjustment of operating parameters.

Table 4-2 represents the cost comparison of restaurant wastewater treatment with two current densities that were applied to wastewater treatment system. It was found that the increasing of current density from 5 to 10 mA/cm^3 decreases TOC and COD removal efficiency of the system because the increase of cell voltage which causes the anodic side

reaction. Furthermore, the increase of cell voltage leads to the power requirement of the system. Consequently, the operating costs of restaurant wastewater treatment are 109 and 303 baht/m^3 when the current densities are 5 and 10 mA/cm^3, respectively.

Table 4-3 presents the operating cost with a variation of residence time. The TOC and COD removal efficiency with the residence time of 3 hr was 62% and the efficiency was 55% with residence time of 2 hr. However, the operating costs were 66 and 109 baht/m^3 when the residence time were 2 and 3 hr, respectively.

Table 4-4 presents the effect of the thickness of SnO_2 active layer on operating cost. It shows that the thickness of SnO_2 active layer has no effect on the operating cost. However, increasing twice SnO_2 thickness may increase the investment cost of electrode.

This study was based on a small reactor of 18 ml. With the small laboratory scale therefore the treatment cost per unit volume of solution may be excessively high. The actual cost of treatment in the large-sized system should be reasonably reduced per unit volume.

Table 4-2 Effect of current density on restaurant wastewater treatment cost by electrochemical oxidation

SnO_2 Thickness (Micron)	Current density (mA/cm^2)	Applied current (A)	Cell voltage (V)	Flow rate (ml/min)	Residence time (hr)	Power required (kW-hr/m^3)	Operating cost (Baht/m^3)	TOC removal efficiency (%)	COD removal efficiency (%)
1.8	5	0.016	16.3	0.10	3	43.5	109	62	62
1.8	10	0.032	22.7	0.10	3	121.1	303	47	47

Table 4-3 Effect of residence time on restaurant wastewater treatment cost by electrochemical oxidation

SnO_2 Thickness (Micron)	Current density (mA/cm^2)	Applied current (A)	Cell voltage (V)	Flow rate (ml/min)	Residence time (hr)	Power required (kW-hr/m^3)	Operating cost (Baht/m^3)	TOC removal efficiency (%)	COD removal efficiency (%)
1.8	5	0.016	14.9	0.15	2	26.5	66	55	54
1.8	5	0.016	16.3	0.10	3	43.5	109	62	62

Table 4-4 Effect of SnO_2 thickness on restaurant wastewater treatment cost by electrochemical oxidation

SnO_2 Thickness (Micron)	Current density (mA/cm^2)	Applied current (A)	Cell voltage (V)	Flow rate (ml/min)	Residence time (hr)	Power required ($kW\text{-}hr/m^3$)	Operating cost ($Baht/m^3$)	TOC removal efficiency (%)	COD removal efficiency (%)
1.8	5	0.016	16.3	0.10	3	43.5	109	62	62
3.6	5	0.016	16.8	0.10	3	44.8	112	51	50